

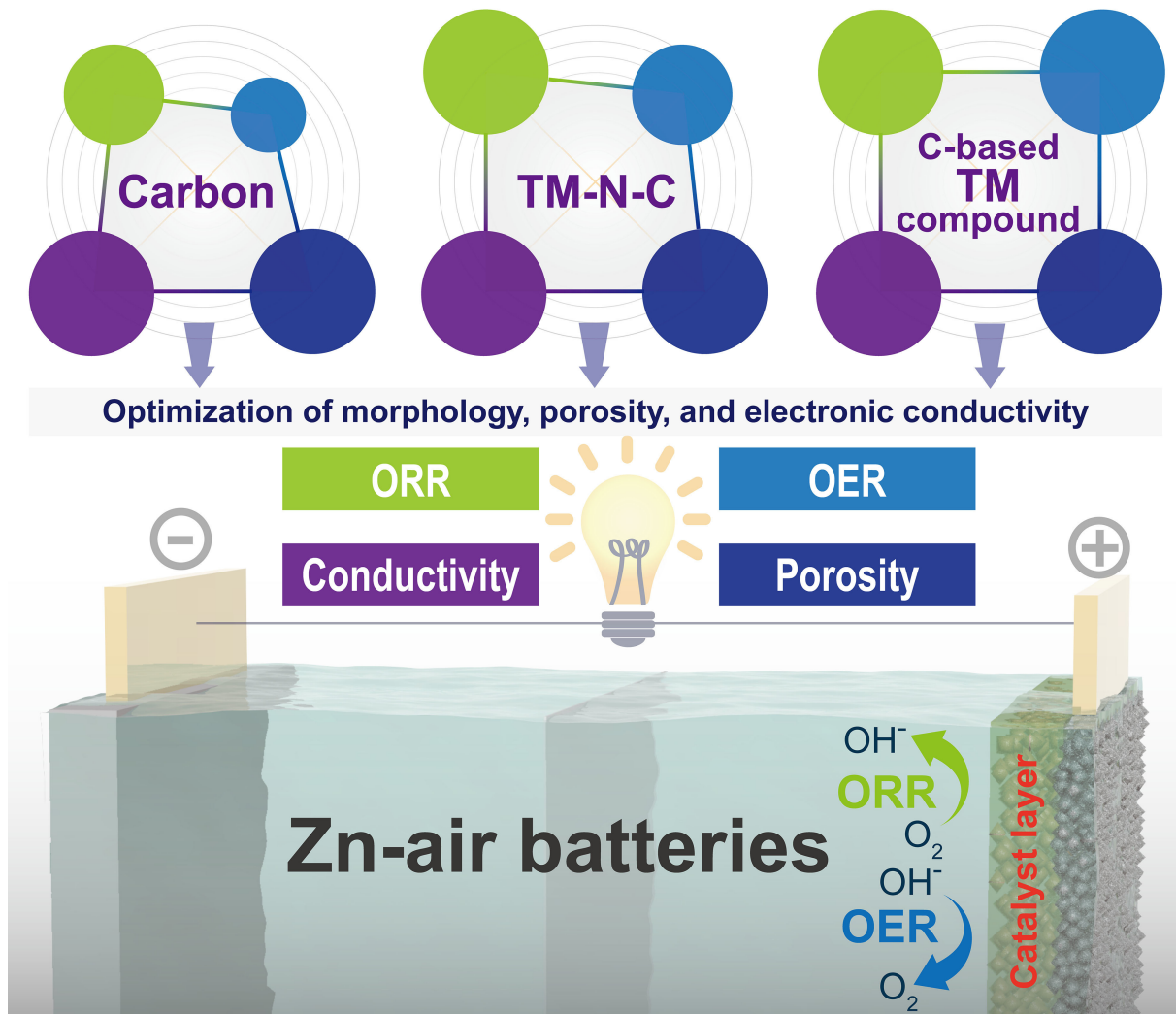
VIP Very Important Paper

Special
Issue

Recent Advances in Metal-Organic Framework Derivatives as Oxygen Catalysts for Zinc-Air Batteries

Yijun Zhong,^[a] Xiaomin Xu,^[a] Wei Wang,^[a] and Zongping Shao^{*[a, b]}

Rational design of MOF-derived catalysts



Electrochemical energy storage systems with high power output, large energy density, and stable performance are urgently needed. Zn-air batteries are one of the most promising candidates owing to abundant and inexpensive resources used, decent energy density, and the high reduction potential of Zn. The most significant challenge of primary and rechargeable aqueous Zn-air batteries is the relatively high overpotential due to the sluggish kinetics of oxygen reactions on the air cathode. Highly efficient oxygen catalysts derived from metal-organic framework (MOF) precursors have demonstrated remarkable capabilities for facilitating the oxygen reactions. In this contribution, we review the recent progress in state-of-the-art MOF-

derived materials for use as oxygen catalysts in primary and rechargeable Zn-air batteries. We first summarize the development of several important MOF derivatives, including transition metal–nitrogen–carbon (TM–N–C) composites, carbon-based transition metal compounds, and metal-free carbons. The advantages and disadvantages of these MOF-derived catalysts are also discussed. Strategies for optimization of the gas–liquid diffusion and the long-range electronic transportation on the air cathode with these MOF-derived catalysts are also demonstrated. Finally, the main challenges and some perspectives for developing advanced MOF-derived catalysts applied in Zn-air batteries are provided.

1. Introduction

Over the past decades, the application of electrochemical energy storage and conversion systems has mitigated the demand and consumption of traditional fossil fuels.^[1] With higher energy conversion efficiency and more simple mechanical configuration, electrochemical batteries, especially, Li-ion batteries, have successfully achieved practical application in portable devices since the 1990s.^[2] In the early 21st century, the rapid technical development of electric vehicles and large-scale smart grids requires more powerful and stable electrochemical energy storage systems.^[3] Batteries with high power output, large energy density, long lifespan and stable performance are urgently needed. Due to the abundant oxygen content in earth atmosphere, metal–air battery can be theoretically fueled by ambient air directly.^[4] Without a solid active material loaded in the cathode, the weight and capacity of a metal–air battery are only based on the metal anode.^[5] Therefore high capacities and energy densities could be achieved. A variety of options like Li, Na, K, Mg, Al, Mn, Fe, and Zn show potential as a metal anode,^[6] among which Li and Zn are the most promising anodes and have attracted most of the interests in the past decades.^[7,8] Li shows a high theoretical specific energy of 5928 Wh kg⁻¹ and a high working voltage of 2.96 V working with an oxygen cathode.^[9] Unfortunately, the highly reactive Li metal may easily react with moisture in the air, thus requiring a protective inert atmosphere during battery fabrication and testing.^[10,11] In

addition, most of the Li–air(O₂) batteries operate in expensive and highly flammable organic electrolytes.^[10,12] These facts hinder the further development and practical application of Li–air(O₂) batteries. Compared to the organic electrolytes, aqueous electrolytes are usually more economical, more eco-friendly, and provide better ionic conductivity.^[13] Due to the abundant and inexpensive resource, decent energy density (1218 Wh kg⁻¹), and higher reduction potential than other metal candidates, Zn could be a more promising metal anode.^[14] In addition, the suitable working voltage (~1.66 V) of Zn–air batteries is just high enough for practical utility and not too high to trigger the decomposition of water in aqueous electrolytes.^[9] Moreover, Zn–air batteries have remarkable advantages such as low capital cost, flat discharge profile, and intrinsic safety in the process of fabrication, operation, and disposal.^[13]

Primary Zn–air batteries are commercially available and widely used for portable applications such as hearing aids and portable data loggers.^[15] Benefiting from the mature practical applications, further development of novel primary and rechargeable Zn–air batteries with better energy output by lowering the discharge/charge overpotentials is more feasible compared to other metal–air battery systems.^[14] Although the reaction between Zn and O₂ are thermodynamically spontaneous, the oxygen reduction reaction (ORR) at the cathode has sluggish kinetics during the battery discharge, which requires the participation of catalysts to accelerate this process.^[16] On the other hand, efficient catalysts for the oxygen evolution reaction (OER) are essential for achieving reasonable charging potential of rechargeable Zn–air batteries.^[17,18] Based on these considerations, the rational design of air cathode is a key determining factor for realizing high-efficient Zn–air batteries.^[18,19] In addition, compared to the inexpensive Zn and electrolyte components, air cathode is considered as the most expensive component in the Zn–air batteries.^[20] Substantial efforts have been made for developing new ORR and OER catalysts, especially in the past 5 years.^[21] Noble metals like Pt, Ir, and their composites show the best catalytic effect.^[22,23] However, from an economic point of view, inexpensive alternatives such as transition metal oxides,^[24,25,26] layered metal hydroxides,^[27] perovskites,^[28] transition metal sulfides,^[29] transition metal nitrides,^[30] transition metal phosphides,^[31] transition

[a] Y. Zhong, X. Xu, Dr. W. Wang, Prof. Z. Shao
WA School of Mines: Minerals
Energy and Chemical Engineering (WASM-MECE)
Curtin University
Perth, WA 6845, Australia
E-mail: zongping.shao@curtin.edu.au

[b] Prof. Z. Shao
Jiangsu National Synergetic Innovation Center for Advanced Materials (SICAM)
State Key Laboratory of Materials-Oriented Chemical Engineering
College of Chemical Engineering
Nanjing Tech University
No. 5 Xin Mofan Road, Nanjing 210009, P.R. China.

Supporting information for this article is available on the WWW under
<https://doi.org/10.1002/batt.201800093>

An invited contribution to a Special Issue on Bifunctional Catalysts for Metal-Air Batteries

metal carbides^[32] and heteroatoms doped metal-free carbons^[33,34] are more favorable.

Metal-organic frameworks (MOFs, also called coordination polymers) are a series of crystalline materials with well-defined structures, remarkable specific surface area, high pore volume and well-dispersed metal nodes on an atomic scale.^[35] Owing to these unique characteristics, MOFs and MOF-derived materials have attracted great considerable attention to be utilized as functional materials for many electrochemical energy storage systems like lithium-ion batteries, lithium-sulfur batteries, supercapacitors,^[26,36] and in energy conversions based on electrocatalysis like the ORR, OER, hydrogen evolution reaction (HER) and carbon dioxide reduction.^[37,38] In recent years, emerging works on MOF-derived catalysts have demonstrated their unique compositional and morphological benefits for use as ORR/OER catalysts in Zn-air batteries. The improved battery performance observed on these MOF-derived oxygen catalysts originates not only from their intrinsically good reactivity for the ORR and OER, but also from other aspects such as enhanced gas and ionic diffusion and optimized electronic conductivity.

Some previous reviews have well summarized recent development on various types of mono-and bi-functional oxygen catalysts, liquid- and solid-state electrolytes, and novel flexible battery configurations for primary and rechargeable Zn-air batteries.^[8,19,39,40,41] Some other reviews have mentioned the use of MOF-derived catalysts for Zn-air batteries.^[14,16,19,20,23,38,42] Up to now, a review that systematically summarizes the exciting progress of MOF-derived material as oxygen catalysts for Zn-air batteries is still in great demand. In this review, we first demonstrate the battery configuration and essential mechanisms of the ORR and OER on the air cathode. In the following, challenges and resolutions for the state-of-the-art MOF-derived catalysts for primary and rechargeable Zn-air

batteries are discussed. The advantages and disadvantages of three types of MOF-derived catalysts (i.e., transition metal-nitrogen-carbon (TM–N–C) composites, carbon-based transition metal compounds, and metal-free carbons) are illustrated. Strategies for optimization of the gas-liquid diffusion and the electronic transportation of the Zn-air batteries with MOF-derived air cathodes are also summarized. At the end of this contribution, perspectives for developing advanced MOF-derived catalysts applied in Zn-air batteries are provided.

2. Battery Configuration and Reaction Mechanism of Air Cathodes

2.1. Configuration of Zn-Air Batteries

As shown in Figure 1, a typical Zn-air battery working in aqueous alkaline electrolyte is composed of a metal Zn anode,

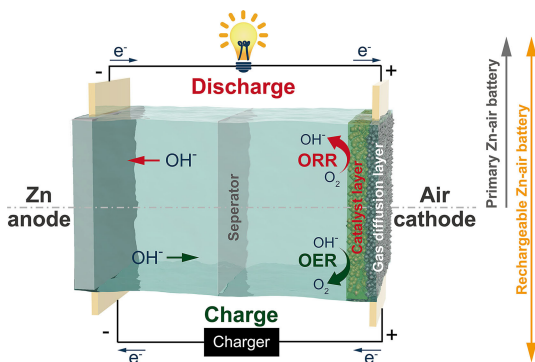
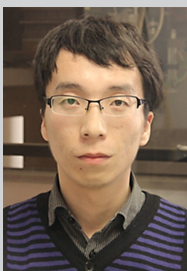


Figure 1. Configuration and discharge-charge process of a Zn-air battery.



Yijun Zhong is now a PhD student in Chemical Engineering at Curtin University. He received his Bachelor (2013) and Master (2016) degrees in Chemical Engineering from Nanjing Tech University, China. His research is focused on developing functional materials for advanced energy storage and conversion systems. His primary interests lie in understanding the effect of structure, composition and morphology on electrochemical performance.



Wei Wang is a research fellow at Curtin University, Australia. He obtained his Ph.D. degree in Chemical Engineering at Nanjing Tech University, China, in 2013. His research interests include anode catalytic materials and coke formation mechanism for solid oxide fuel cells (SOFCs) operating on hydrocarbons, fuel selection and application for SOFCs, photocatalysts for the degradation of organic substances, photoanodes and photocathodes for dye-sensitized solar cells (DSSCs) and light absorbers for perovskite solar cells.



Xiaomin Xu is now pursuing a Ph.D. degree in Chemical Engineering at Curtin University, Australia. He received his Bachelor (2013) and Master (2016) degrees in Chemical Engineering from Nanjing Tech University, China. His research interests include the structure, synthesis, and characterization of perovskite materials and their application in electrocatalysis, including the oxygen reduction reaction, oxygen evolution reaction, and hydrogen evolution reaction.



Zongping Shao is a professor of chemical engineering at Curtin University, Australia and Nanjing Tech University, China. He obtained his PhD from Dalian Institute of Chemical Physics, China in 2000. He worked as a visiting scholar at Institut de Recherches Sur La Catalyse, CNRS, France and postdoc at California Institute of Technology, USA from 2000 till 2005. His current research interests include solid-oxide fuel cells, lithium-ion batteries, oxygen-permeable membranes and low-temperature energy-conversion devices.

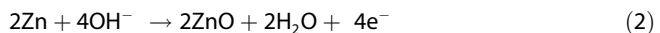
electrolyte, a separator, and an air cathode. In some research, a three-electrode configuration with one Zn electrode and two functional air electrodes (one for oxygen reduction and the other for hydroxide reduction) is adopted.^[19] We only demonstrate the model of the two-electrode battery here since most of the batteries with MOF-derived cathodes are investigated based on this configuration. The aqueous liquid electrolyte offers a medium for fast ionic conductivity via diffusion. A most adopted electrolyte for aqueous primary and rechargeable Zn-air batteries are alkaline 6 M KOH, which offers an ionic conductivity of 620 mScm⁻¹.^[20] In some investigations for rechargeable Zn-air batteries, low concentration (e.g., 0.2 M) of ZnCl₂ or Zn(Ac)₂ are added into the electrolyte to facilitate the reversible conversion of Zn anode.^[43]

The Zn anode is usually in the form of pure Zn plate or Zn powder loaded on conductive supports.^[41] The air cathode usually comprises a gas diffusion layer and a catalyst layer. Typically, the gas (oxygen) diffusion layer is composed of active carbon and highly-hydrophobic polytetrafluoroethylene.^[44] This allows the of oxygen and prevents the leakage of water in the electrolyte.

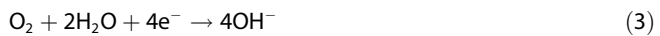
The overall electrochemical reaction in a primary Zn-air battery can be illustrated as:^[8,40]



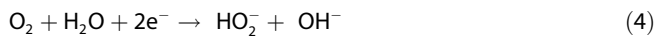
During discharge, the Zn anode is oxidized and reacts with hydroxide ions to produce Zn(OH₄)²⁻, then further decomposes to ZnO.^[14] This transformation follows the reaction:



In cathode, oxygen is reduced at the three-phase-boundary of catalyst-oxygen-electrolyte. In most cases, the reduction reaction follows a four-electron reaction process.^[20]



At the same time, unfavorable superoxide may be produced via a two-electron process of oxygen reduction.^[20]



Competition of the four-electron and two-electron processes is highly associated with the selectivity of the catalyst.^[14] As we will discuss in the next section, ORR catalysts with high four-electron selectivity are critical for achieving high energy density and working efficiency.^[19]

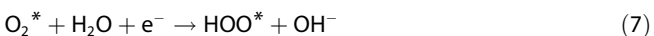
The above reaction processes are irreversible in a primary Zn-air battery, where the ORR activity of the catalysts has a major impact on the performance of the batteries. For a rechargeable Zn-air battery, ZnO can transform backwards stepwise and is deposited as metal Zn on the surface of the anode.^[14] During charging process, hydroxide ions are re-oxidized with the aid of catalysts via a four-electron OER process under the outer power supply.^[20]



In this case, bifunctional catalysts capable of catalyzing both the ORR and OER are indispensable for realizing a high-efficient rechargeable zinc-air battery.

2.2. Mechanism for the Oxygen Reduction and Oxygen Evolution Reaction

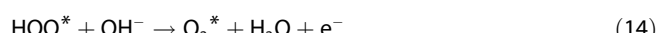
In aqueous alkaline solutions, the electrochemical reduction of oxygen has rather sluggish kinetics, even with the involvement of an electrocatalyst. Generally, the ORR in the air electrode of a zinc-air battery proceeds via the following steps: i) oxygen diffuses through the gas diffusion layer and adsorbs on the catalyst surface; ii) oxygen accepts electrons transferred from the zinc anode and is reduced at the catalyst/oxygen interface; and iii) the reduction product desorbs from the catalyst surface and transfers through the electrolyte to the zinc anode.^[45] Regarding the exact reaction mechanism of the ORR, two major reaction pathways have been observed in alkaline media over the past decades. One is an indirect two-electron pathway that produces an intermediate product of peroxide, which is considered unfavorable due to the corrosive nature of peroxide that can cause low energy efficiency and instability of the electrochemical cell.^[13,46] The other is a direct four-electron pathway and is considered to be the preferable pathway. Despite the different ORR pathways on different catalysts surfaces and under different experimental conditions, one typical mechanism for the ORR, which has been reported for metal and metal-based catalysts,^[47,48] involves the formation of several oxygenated adsorbates including O₂^{*}, HO^{*}, O^{*}, and HO^{*} (* denotes a surface active site) as shown below.



The generation of these oxygen adsorbates plays a decisive role in determining the catalyst performance. According to the Sabatier principle, an optimum catalytic activity is expected when the oxygen species bind to the catalyst surface neither too strongly nor too weakly.^[49] Therefore, accessing the binding energies of the different oxygen intermediates is important to the identification of the rate-determining step of the overall ORR. This, however, remains difficult to accomplish experimentally, and has been possible via computational methods.^[47,50]

The evolution of oxygen in alkaline water is also a complex process, whose reaction mechanism differs according to the catalyst materials and active sites.^[24] A generally accepted OER reaction pathway comprises four consecutive proton and electron transfer steps, where a sequence of oxygen adsorbates

is generated including HO^* , O^* , HOO^* , and O_2^* . This actually is a reverse version to the ORR pathway as mentioned above.



This mechanism is mainly revealed on oxide surfaces as well as oxidized metal surfaces.^[51] Analogous to the ORR, the OER reaction kinetics are largely controlled by the binding strength of adsorbed oxygen species on the reactive surface sites. Theoretical calculations suggest that a universal scaling relationship is present between the binding energies of HO^* and HOO^* species,^[52] where too weak of an oxygen binding strength renders the oxidation of HO^* being rate-determining whereas too strong of an oxygen binding strength leads to the formation of HOO^* being rate-limiting. This further gives rise to a general activity descriptor, ($\Delta G_{\text{O}_2} - \Delta G_{\text{HO}^*}$), which correlates the OER activity with the difference of binding energies between two oxygen intermediates. Understanding these relations can help design active oxygen electrocatalysts. Note that other classes of catalyst materials may obey a different relation between adsorption strength.

3. MOF-Derived Catalysts for Zn–Air Batteries

As presented in Figure 2, most of the MOF-derived oxygen catalysts reported to date are carbon-based materials with remarkable electronic conductivity and porosity. Three types of the MOF-derived materials show different activities for the ORR and OER. The benefits and drawbacks of these materials and design methodologies are also indicated in the figure. It is worth mentioning that both the activity for oxygen catalysis

and the transfer efficiency for gas, ion, and electron are important for the resulting Zn-air battery performance. Based on this clue, most of the important physical properties (i.e., Brunauer-Emmett-Teller specific surface area (a_{BET})), ORR and OER activity evaluation parameters (e.g., half-wave potential for the ORR ($E_{1/2}$)), number of electrons transferred for the ORR (n) and potential for a geometrical current density of 10 mA cm^{-2} for the OER ($E_{j=10}$)), as well as battery performance (e.g., open circuit voltage (OCV), charge voltage (V_C), discharge voltage (V_D), peak power density (PPD), specific capacity and durability) are summarized and compared in Tables S1 and S2.

3.1. Transition Metal–Nitrogen–Carbon Composites

In 2016, Xia et al. proposed a strategy that converted MOF (Co-ZIF-67, here ZIF is the abbreviation for zeolitic imidazolate framework) into a highly graphitized hollow framework composed of Co particles decorated N-doped CNT frameworks (NCNTFs, Figure 3a).^[53] A hollow structure with a void and N-doped CNTs framework shell (Figure 3b–c) is generated after calcination of the ZIF precursor. The catalyst exhibited excellent ORR/OER performance. For example, the half-wave potential of the NCNTFs catalyst is superior to commercial Pt/C electrocatalyst (Figure 3d). This work has later inspired the development of a series of MOF-derived TM–N–C composites for application in Zn-air batteries.

3.1.1. Transition Metals

Co–N–C materials are well studied as mono-functional catalysts for primary Zn-air batteries and as bifunctional catalysts for rechargeable Zn-air batteries. Most Co–N–C catalysts applied in Zn-air batteries are synthesized using ZIF-67 precursor.^[54–59] For example, a Co embedded N-doped carbon polyhedron by directly calcinating ZIF-67 at 800°C under a N_2 flow is proposed by Li et al.^[57] Zhang et al. developed Co particles encapsulated N-doped CNTs by a solid thermal reaction of dicyandiamide ZIF-

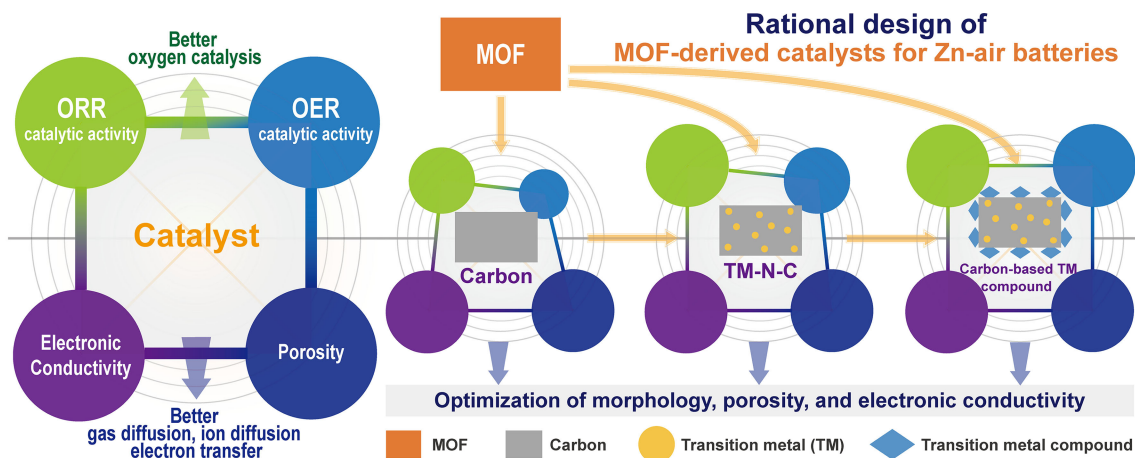


Figure 2. Illustration of the developing strategies of MOF-derived oxygen catalysts and their advantages.

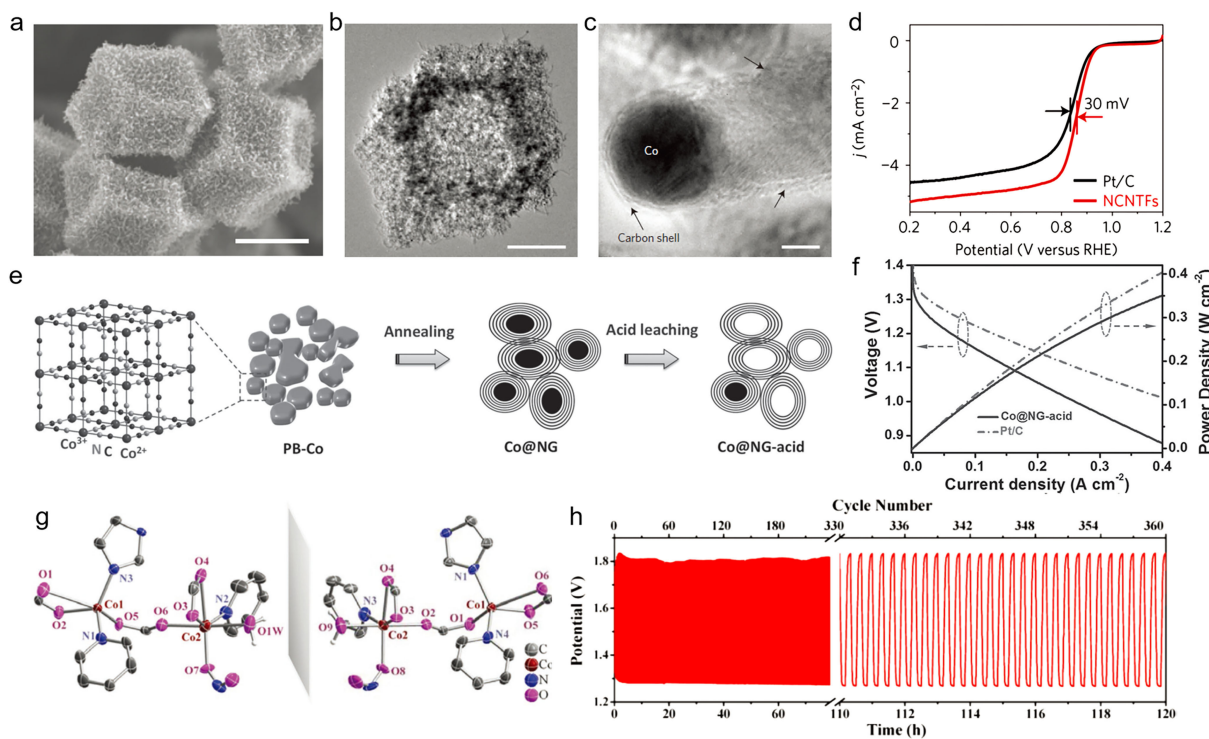


Figure 3. a) Scanning electron microscope (SEM) image, b) Transmission electron microscopy (TEM) image, c) high-resolution transmission electron microscopy (HR-TEM) image of highly graphitized hollow framework composed of Co particles decorated N-doped CNT frameworks (NCNTFs), d) comparison of ORR performance of Pt/C and NCNTFs in 0.1 M KOH. e) synthetic process of Co nanoparticle encapsulated N-doped graphene (Co@NG-acid), f) electrochemical performance of primary Zn-air batteries with Co embedded N-doped graphene shell (Co@NG-acid) and Pt/C oxygen catalysts. g) Mirrored symmetrical coordination feature of the Co-MOF precursor, h) cycling of rechargeable Zn-air batteries with C-MOF-C2-900 derived from the Co-MOF. Reprinted with permission from (a)–(d)^[53] Copyright 2016 Springer Nature, (e), (f)^[63] Copyright 2016 WILEY-VCH Verlag GmbH & Co. KGaA, Weinheim, (g), (h)^[64] Copyright 2018 WILEY-VCH Verlag GmbH & Co. KGaA, Weinheim.

67.^[54] Some other works on ZIF-67 introduced functional additives during the synthesis process to construct a CNT framework via catalytic reforming of the MOF precursor. We will further discuss these optimizations for the Co–N–C based composites in Section 3.4.

ZIF-8 and ZIF-67 have the same organic imidazolate ligand and a similar structure. The major difference of ZIF-8 and ZIF-67 is their different coordinated metals (i.e., ZIF-67 has a Co node and ZIF-8 has a Zn node). To obtain improved porosity of the Zn, Co coexisted ZIF or a core-shell ZIF-8@ZIF-67 as precursors.^[43,60–62] For example, Zhang et al prepared Co–N–C material for primary Zn-air batteries from Zn,Co-ZIF with different Zn:Co molar ratios.^[61] They found that a_{BET} of the resulting Co–N–C materials increases with the increasing proportion of Zn. Wang et al designed a ZIF-8@ZIF-67 composite which produced a Co–N–C material with highly porous N-doped carbon cores and highly graphitized Co–N–C shells.^[43] The core-shell Co–N–C material exhibited higher ORR activity than that of the materials derived from ZIF-8 or ZIF-67 precursor, as well as better performance for Zn-air batteries. Wang et al. reported a Co nanoparticles embedded N-doped CNTs by calcinating a 2D leaf-like Zn,Co-ZIF precursor.^[65] The bifunctional catalyst demonstrated great performance of rechargeable Zn-air batteries both in the two-electrode and the three-electrode configuration. Amiinu et al. proposed a novel strategy to synthesize Co–N–C materials with high porosity by post-coordination of

Co.^[66] The Co–N–C material obtained from this strategy demonstrated better ORR and OER activity than Pt/C and IrO₂, respectively. By using an ex-situ X-ray photoelectron spectroscopy (XPS) analysis and density functional theory (DFT) calculation, their work also clarified the coupling effect of Co–N on its excellent ORR activity. Their Co–N–C material demonstrated decent energy density and low overpotentials in primary Zn-air batteries and solid-state rechargeable Zn-air batteries.

Besides ZIF series MOF, other precursors have also been utilized for producing Co–N–C materials.^[63,64,67,68] As illustrated in Figure 3e, Zeng et al. used Co-PBA as a precursor for obtaining highly graphitized carbon shells on the metal Co particles.^[63] By etching most of the metal Co particles with 1 M HCl, the product still contains residual Co in the carbon matrix. An impressively high energy density of 350 mWcm⁻² was demonstrated for primary Zn-air battery with the catalyst after acid etching (Figure 3f). Gao et al. proposed Co clusters embedded N-doped reduced graphene oxide (rGO) by pyrolysis of DUT-58(Co) MOF and graphene oxide (GO) complex.^[67] The well-dispersed, ultra-small Co cluster (~2 nm) on the N-doped rGO provided abundant oxygen adsorption sites, thus facilitating the ORR activity. In addition, the 2D rGO support afforded excellent electronic conductivity. As a result, a remarkable high-rate performance at 300 mA cm⁻² was achieved. Very recently, Zhang et al. designed a Co–N–C material with a rod-like

morphology from a pair of enantiotopic chiral 3D MOFs (Figure 3g).^[64] The Co–N–C material presented outstanding bifunctional catalytic capability. Impressively, discharge and charge potentials of 1.28 and 1.81 V, respectively, were achieved at 2 mA cm^{-2} throughout the 360-cycle in 120 h (Figure 3h). This result is one of the best records among advanced rechargeable Zn–air batteries with MOF-derived catalysts.

Except for Co–N–C composite, other TM–N–C catalysts (e.g., Fe–N–C^[69,70,73–75] and Cu–N–C^[76]) have also been inves-

tigated. As illustrated in Figure 4a, Ahn et al. proposed a Te metal template-assisted synthesis of hierarchically porous Fe–N–CNTs composite,^[69] which gave rise to a highly interconnected 1D structure (Figure 4b) with a high α_{BET} value of $1380 \text{ m}^2 \text{ g}^{-1}$. The composite was applied as a mono-functional catalyst in one of the air cathodes for rechargeable batteries. To obtain better charging performance, the same authors utilized NiFe LDH/NiF composite catalyst as an additional air cathode. Batteries with this decoupled configuration demonstrated a

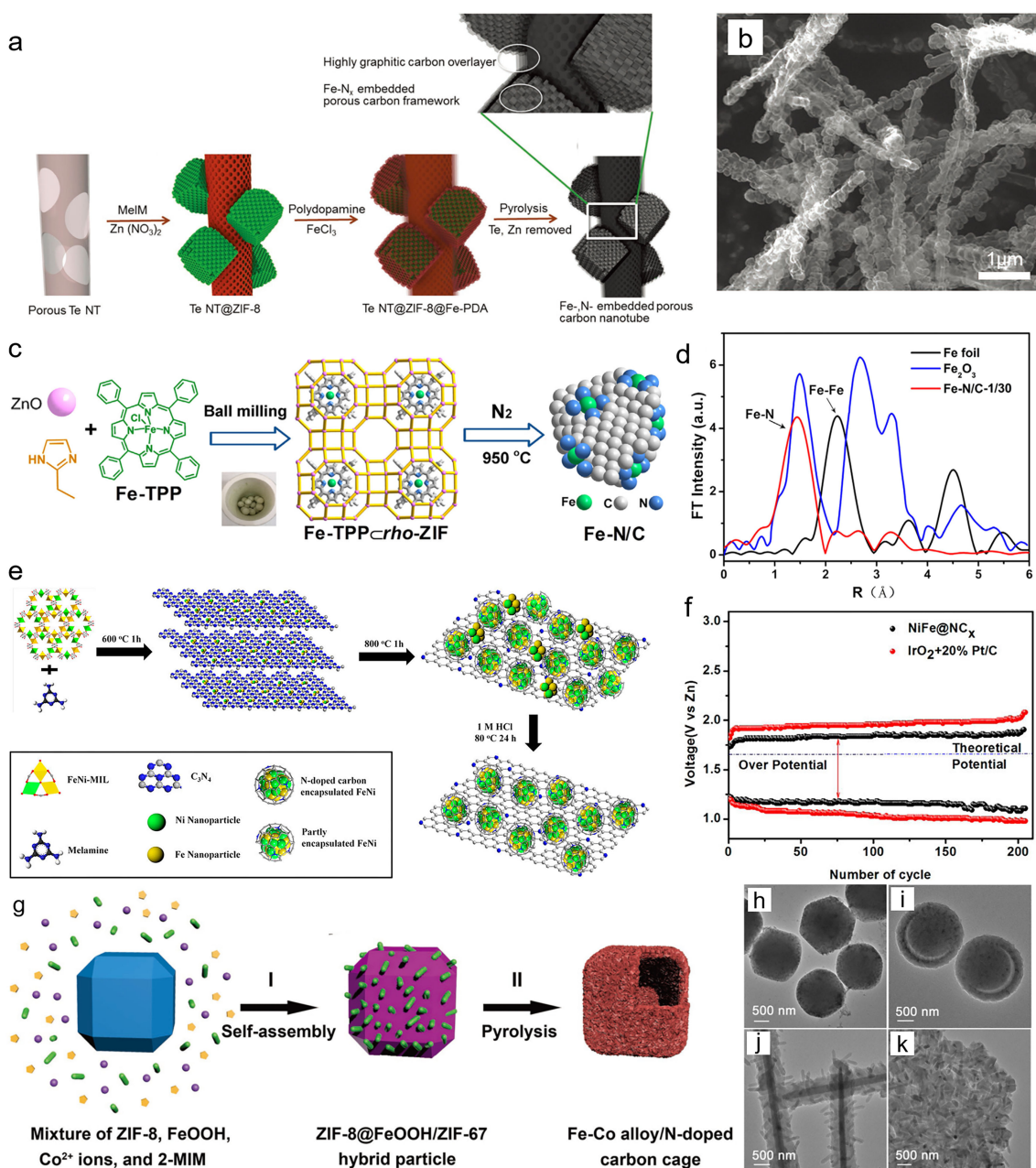


Figure 4. a) Illustration of the synthetic process for Fe–N–CNTs composite, b) SEM image of the Fe–N–CNTs; c) Illustration of the synthetic strategy for Fe–N/C catalyst with single-atom Fe, d) Fourier-transformed Fe K-edge XANES spectra of the Fe–N/C material; e) Illustration of the synthesis procedures of the NiFe@NC_x composite, f) comparison of cycling performances of rechargeable Zn–air batteries with NiFe@NC_x and IrO₂ + 20Pt/C catalysts; g) Illustration of the synthetic strategy of porous Fe–Co alloy/N-doped carbon cages, TEM images of h) ZIF-8@FeOOH/ZIF-67 hybrid particles, i) polystyrene@FeOOH/ZIF-67 hybrid spheres, j) MoO₃@MIL-88/ZIF-67 hybrid rods, k) GO@MIL-88/ZIF-67 hybrid sheets. Reprinted with permission from (a), (b)^[69] Copyright 2017 WILEY-VCH Verlag GmbH & Co. KGaA, Weinheim, (c), (d)^[70] Copyright 2018 Elsevier, (e), (f)^[71] Copyright 2016 American Chemical Society, (g)–(k)^[72] Copyright 2018 WILEY-VCH Verlag GmbH & Co. KGaA, Weinheim.

voltage gap of only 0.58 V. Ma et al. developed a compressible and bendable Zn-air battery with a bifunctional catalyst which composed of single-site dispersed Fe–N_x on 2D porous N-doped carbon layer.^[75] The batteries exhibited excellent performance with a conventional aqueous electrolyte. With solid-state electrolyte configuration, the batteries demonstrated decent performance even under 54% compression strain or under 90° bend condition. A novel strategy for synthesizing single-atom Fe decorated N-doped carbon was designed by Wei et al (Figure 4c).^[70] They confirmed the single-atom distribution of Fe with X-ray absorption near edge structure (XANES) spectra (Figure 4d). The single-atomic scale dispersion of Fe showed a promising improvement on ORR catalysis. Primary Zn-air batteries with the single-atom catalyst demonstrated excellent discharge voltages of 1.4 V at 2 mA cm⁻². A Cu–N–C composite was obtained using a Cu-doped ZIF-8 precursor,^[76] which displayed improved ORR activity and decent battery performance due to the well-tuned Cu–N structure.

3.1.2. Transition Metal Alloys

In 2016, Zhu et al. indicated that the intrinsic activity of TM–N–C composites is dependent not only on the TM–N sites and the doped N atoms, but also on the electronic structure of the surface carbon.^[71] The electronic structure can be optimized via the modulation effect from the TM core. A Fe, Ni encapsulated N-doped graphene was prepared by calcination of a mixture of FeNi-MIL with melamine (Figure 4e). NiFe@NCx catalyst with FeNi alloy had a better tuned electronic structure of the nearby carbon atoms on the wrapped graphene, thereby contributing to improved ORR and OER activity relative to TM–N–C composites with only Fe or only Ni as a metal core. The bifunctional NiFe@NCx catalyst was tested for rechargeable Zn-air batteries and demonstrated comparable performance to a IrO₂ + 20%Pt/C catalyst (Figure 4f).

TM–N–C composites containing other alloys like CoFe were designed in the following research.^[77–79] By coating a Fe-based NH₂-MIL-88B MOF with ZIF-67, a CoFe encapsulated N-doped carbon polyhedron was fabricated after calcination of the dual MOFs. In another work, Cai et al. proposed a core-shell structured CoFe–N–C composite from a Co–Fe PBA.^[78] In addition, Wang and coworkers designed a Cu particle encapsulated Fe–N–C composite from a FeCu-ZIF.^[80] Owing to the uniform dispersion of Cu and Fe atoms in the MOF-derived composite, excellent ORR performance was observed with an E_{1/2} value of 0.982 V. The Cu@Fe-N-C catalyst presented decent performance and good durability in primary Zn-air batteries.

In a recent work proposed by Ling et al., a Zn and Co embedded N-doped carbon fiber also demonstrated better ORR reactivity compared to catalysts with only Zn or Co present in the N-doped carbon fiber.^[81] By comparing the ORR activity after poisoning the transition metal (Zn and Co) using 2, 2'-bipyridine (Bpy), the authors found that the introduction of Zn further promoted the activity of the active N sites. When evaluated in a primary Zn-air battery, the Zn and Co embedded

carbon fiber catalyst showed enhanced energy density in comparison to the carbon fiber with only Zn or Co.

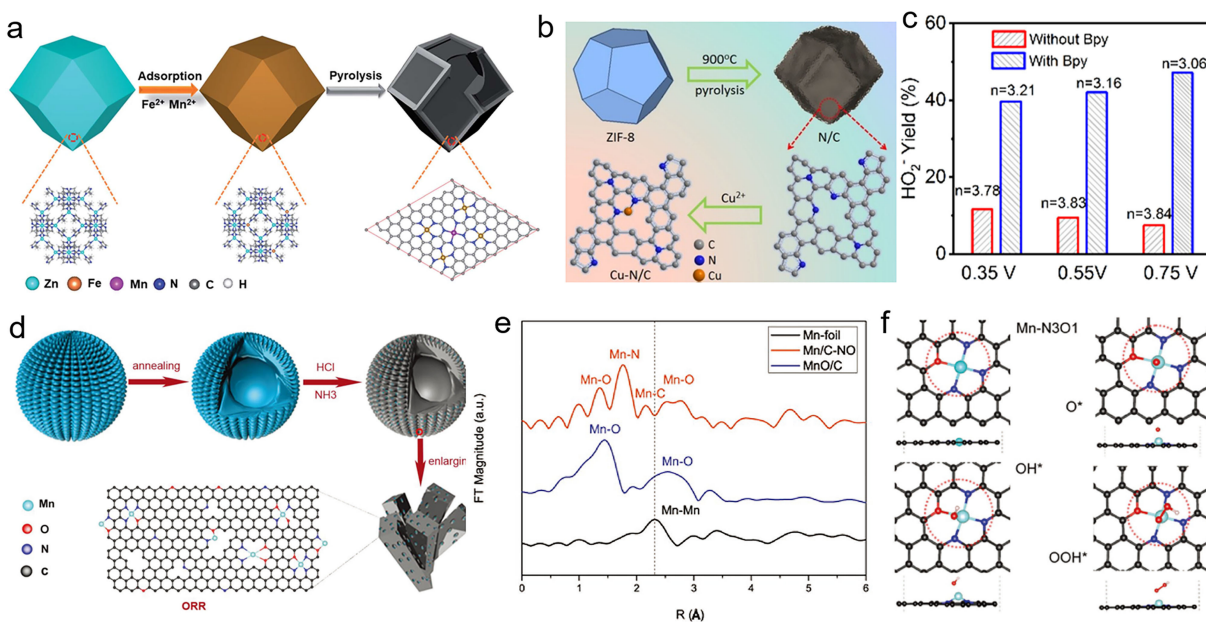
In a recent work, Lou and co-workers proposed a general strategy for developing ZIF-67 based hybrid materials.^[72] As illustrated in Figure 4g, ZIF-8@FeOOH/ZIF-67 hybrid particles were synthesized by self-assembling of ZIF-67 and FeOOH nanorods on a ZIF-8 support (Figure 4h). After calcination, the resulting Fe–Co alloy/N-doped carbon cage demonstrated excellent ORR activity which was superior to Pt/C catalyst. Based on the strategy, other ZIF-67-based complexes were also proposed based on various supports like polystyrene spheres (Figure 4i), MoO₃ rods (Figure 4j) and GO sheets (Figure 4k). Lou's work provides a new toolbox for developing MOF and derived materials as electrochemical catalysts for Zn-air batteries.

3.1.3. Single-Atom Catalysts

As mentioned in the last section, single-atom metal provides much improved active sites (in both quantity and quality) for oxygen reactions. In the past few years, intensive research interests have been focused on the role of single-atom metal catalysts in electrocatalysis.^[82] As already illustrated by the example reported by Wei et al.,^[70] calcination of rationally designed MOF precursors would be a promising strategy for preparing carbon-based single-atom metal catalysts. Other preparation strategies have also been developed recently for the acquisition of single-atom catalysts.

Zhang et al. reported single-atom Co confined N-doped carbon flake arrays as oxygen electrocatalysts.^[83] By comparing the ORR and OER activities before and after the removal of the redundant Co clusters, they suggested that the active site for the oxygen reactions is Co–N₄. A rechargeable Zn-air battery with this cathode catalyst showed decent charge and discharge voltages as well as durable cycling performance over 570 cycles within 180 h. The catalyst also demonstrated good performance in a flexible solid-state Zn-air battery. Gong et al. proposed a Fe, Mn–N–C composite with uniformly dispersed Mn and Fe single-atoms.^[84] By using DFT calculations, the authors revealed that the protonation of O* to HO* is the rate-determining step of ORR on Fe, Mn–N–C, which needs a lower energy compared to Fe–N–C and Mn–N–C. Consequently, the single-atom Fe, Mn–N–C catalyst demonstrated better ORR performance than Fe–N–C and Mn–N–C, which even outperformed Pt/C catalyst when used as an air electrode in a primary Zn-air battery. Lai et al. proposed a post-coordination strategy for anchoring single-atom Cu on a N-doped carbon derived from the ZIF-8 precursor (Figure 5b).^[85]

A comparable ORR activity to Pt/C catalyst was observed for the Cu–N–C catalyst. By poisoning the Cu sites with Bpy, ORR activity of the Cu–N–C material dropped significantly (Figure 5c). This result suggested that the Cu–N_x served as the main active sites for ORR. A primary Zn-air battery with this single-atom Cu–N–C catalyst presented a high PPD and a stable long-term performance. These results of the batteries were better than those of the previously reported batteries with



catalysts decorated by Cu particles (as discussed in Section 3.1.1).^[76]

Very recently, the non-negligible role of O atoms in a TM–N–C composite was revealed by Yang et al.^[86] A Mn/C–NO catalyst with evenly dispersed single-atom Mn was prepared from a Mn-BTC precursor (Figure 5d). Fourier transformed Mn K-edge XANES spectra confirmed the bonding of Mn–N and Mn–O in Mn/C–NO (Figure 5e). The coordination effect of both O and N atoms on the nearby single-atom Mn was found to result in the well-tuned d-electron density of Mn atoms, which contributed to the excellent ORR activity observed on Mn/C–NO. Further DFT calculations suggested that the desorption of HO^{*} is the rate-determining step based on a Mn-N₃O₁ model (Figure 5f), which has a low energy uphill close to that of Pt (111), indicating its high reactivity toward the ORR. When tested in a primary zinc-air battery, the Mn/C–NO catalyst delivered higher performance than Pt/C. Yang's work provides a deeper understanding of the single-atom TM catalysts with oxygen- and nitrogen-containing carbon supports.

3.2. Carbon-Based Transition Metal Compounds

While TM–N–C materials are excellent catalysts for the ORR, their OER performance is usually incomparable to other well-studied catalysts such as IrO_x, RuO_x, and CoO_x.^[87] To reduce the overpotential for rechargeable Zn–air batteries, the OER activity of catalysts should be further improved. As illustrated in Figure 6a, besides direct pyrolysis of the MOF precursor under a well-controlled condition,^[88–93] two different strategies have also been developed to obtain metal compounds (e.g., oxides,

sulfides, nitrides and phosphides) from the TM–N–C. One is to convert or partially convert the transition metal particles via thermal reactions.^[94–96] The other is to introduce metal compounds by coating, deposition, or other integration methods.^[97–100]

3.2.1. Metal Oxides and Metal Hydroxides

In 2016, Lee et al. proposed a scalable method for producing Mn_xCo_{3-x}O₄ on a N-doped carbon support.^[88] A relatively low calcination temperature of 400 °C and an air atmosphere were adopted for converting the Co and Mn containing PBA into a highly porous structure. They indicated that the highly porous structure derived from the MOF precursor not only increases the number of active sites for ORR but also facilitates gas transfer. By adding functional reagents (e.g., ZnO, polyacrylonitrile(PAN), and polyaniline(PANI)) to control the carbonization process of MOFs, carbon-based transition metal oxides can be obtained directly from one-step calcination. For example, Chao et al. reported a Co/CoO_x decorated 1D N-doped carbon nanotube structure (Co@CoO_x/NCNTs, Figure 6b and c) by using ZnO nanowires to generate excess O atoms for oxidizing Co.^[89] As demonstrated in Figure 6d, a primary Zn-air battery with this material demonstrated much better rate performance than those with a Pt/C or with a Co–N–C composite. The remarkable discharge potential of 0.69 V at 500 mA cm⁻² was one of the best high-rate results in primary Zn-air batteries using MOF-derived catalysts. Khalid et al. produced a Co/Co₃O₄ encapsulated N-doped carbon by the assistance of PANI.^[90] They found

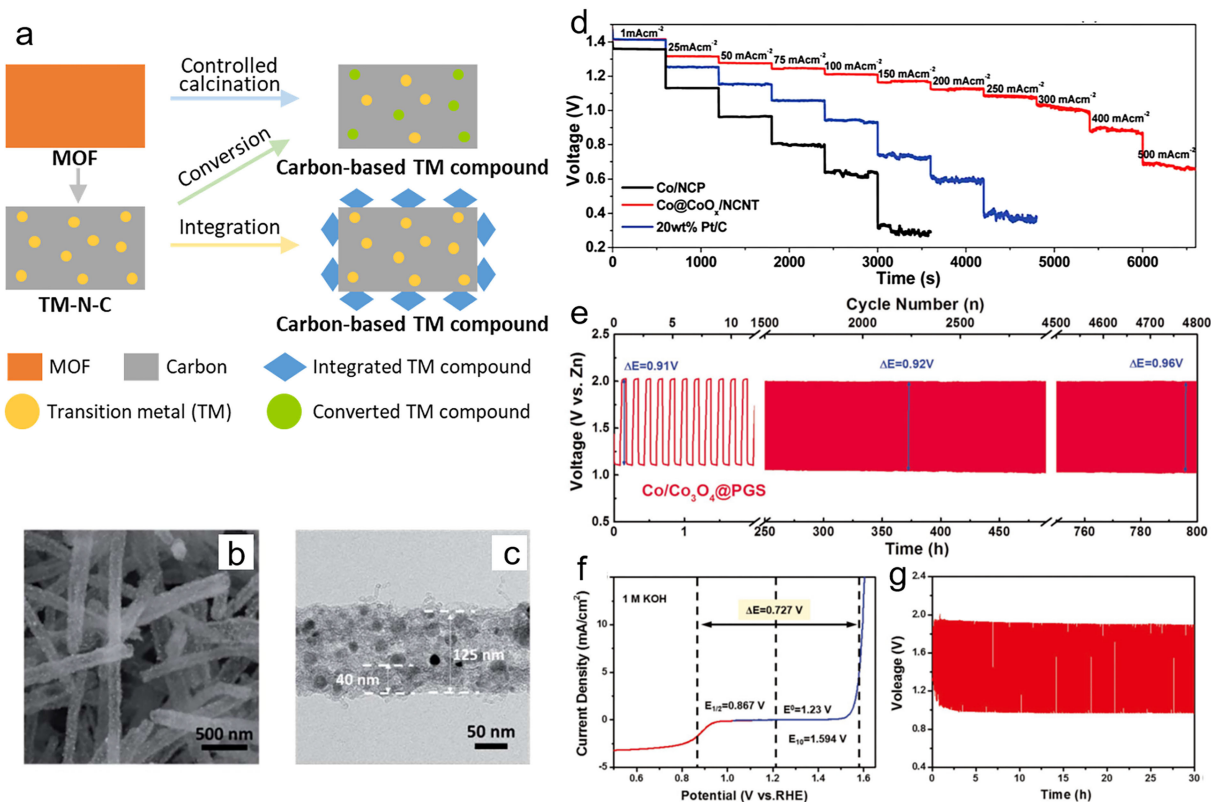


Figure 6. a) Illustration of strategies for obtaining carbon-based transition metal compounds from MOF precursors; b) SEM image and c) TEM image of $\text{Co}@\text{CoO}_x/\text{NCNTs}$; d) Rate performance comparison of primary Zn-air batteries with $\text{Co}@\text{CoO}_x/\text{NCNTs}$ and Pt/C catalyst; e) Cycling stability of a rechargeable Zn-air battery with $\text{Co}/\text{Co}_3\text{O}_4$ @porous graphitized shells (PGS) catalyst; f) Polarization profile of $\text{NiFe-LDH}@/\text{Fe}/\text{carbon nanoplate}$ (CNP) catalyst in 1 M KOH, g) Cycling stability of a rechargeable Zn-air battery with $\text{NiFe-LDH}@/\text{Fe}/\text{CNP}$ bifunctional catalyst. Reprinted with permission from (b)–(d)^[89] Copyright 2017 Royal Society of Chemistry, (e)^[91] Copyright 2018 WILEY-VCH Verlag GmbH & Co. KGaA, Weinheim, (f), (g)^[99] Copyright 2018 WILEY-VCH Verlag GmbH & Co. KGaA, Weinheim.

the initial amount of PANI has a vital influence on the reduction degree of Co.

Oxidized cobalt compounds like CoO_x and Co_3O_4 are promising bifunctional catalysts. However, the above works did not present the results for rechargeability Zn-air batteries. Jiang et al. recently obtained $\text{Co}/\text{Co}_3\text{O}_4$ porous graphitized shells (PGS) using a one-step pyrolysis, which demonstrated an impressively durable 4800-cycle performance over 800 h in a rechargeable Zn-air battery (Figure 6e).^[91] Guo et al. introduced a post-oxidation process at 300 °C to partially oxidize metallic Co into Co_3O_4 .^[94] The ZIF-67-derived carbon-based Co– Co_3O_4 materials demonstrated excellent performance in rechargeable Zn-air batteries. Wu et al. demonstrated the formation of N-doped carbon decorated by evenly dispersed Co, $\text{ZnxCo}_{3-x}\text{O}_4$, and Co_3O_4 species converted from a $\text{Zn},\text{Co-ZIF}$ precursor.^[101] This multicomponent compound exhibited good bifunctional activity in a rechargeable Zn-air battery.

In some other recent works, the “integration” strategy as illustrated in Figure 6a has been adopted for producing complicated carbon-based transition metal compounds from MOF precursors. For example, Chen et al. prepared a 1D core-shell structured $\text{MnO}@\text{Co-N-C}$ composite using ultrathin α - MnO_2 nanotubes as the template for encapsulating ZIF-67 precursor.^[97]

A rechargeable Zn-air battery with this bifunctional catalyst demonstrated excellent cycling stability over 633 h at 5 mA cm⁻². Li et al. proposed a spinel NiCo_2O_4 decorated Co–N–CNTs nanocage by depositing NiCo-layered double hydroxide (LDH) on the ZIF-67 precursor.^[98] Song et al. developed a series of hollow carbon-based catalysts with Co or Fe nanoparticles encapsulated in 1D, 2D, or 3D morphologies by growing $\text{Zn},\text{Co-ZIF}$ or $\text{Zn},\text{Fe-ZIF}$ on a ZnO template.^[99] The obtained Fe–N–C and Co–N–C nanoplates presented excellent activity for the ORR. NiFe-LDH was further deposited on the Fe–N–C nanoplate via a hydrothermal method to obtain improved activity for the OER. As shown in Figure 6f, the catalyst shows a voltage gap of only 0.727 V between the $E_{1/2}$ and $E_{j=10}$, indicating excellent bifunctional capability. The catalyst was further applied in rechargeable Zn-air batteries, delivering stable discharge and charge voltages over 300 cycles (Figure 6g).

3.2.2. Other Metal Compounds

In 2016, Meng et al. proposed a bifunctional catalyst composed of Co_4N and Co on N-doped carbon derived from a ZIF-67-polypyrrole (ppy) complex.^[92] As illustrated in Figure 7a, the

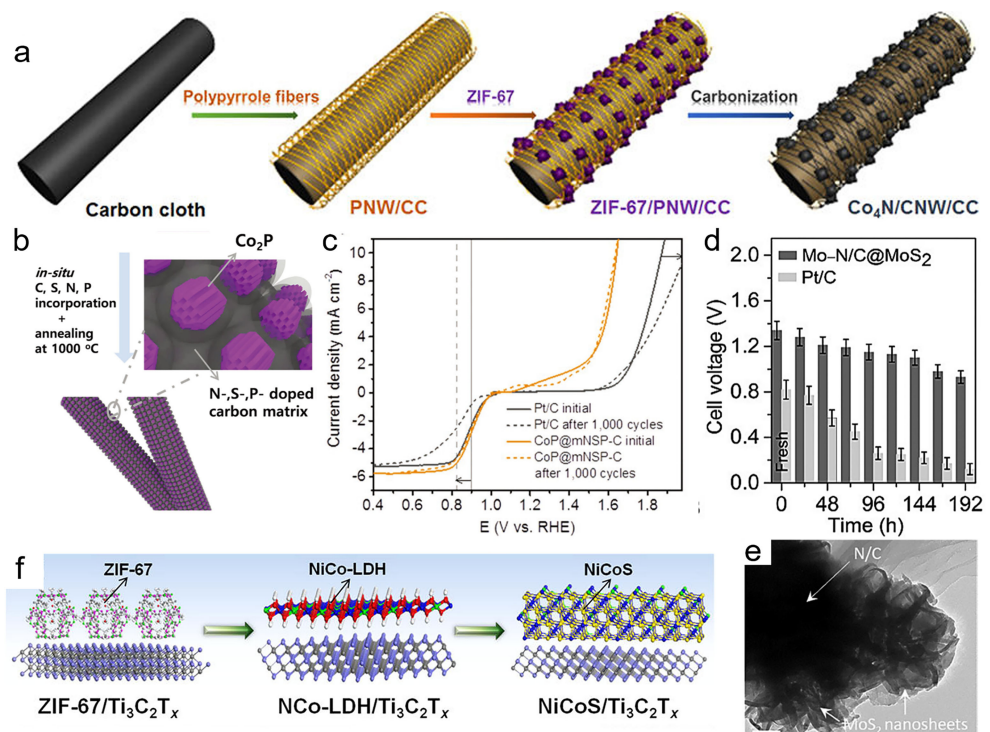


Figure 7. a) Illustration of the synthetic process of Co₄N/CNW/CC; b) Illustration of the preparation process and the morphological structure of CoP@mNSP-C; c) Polarization profiles of CoP@mNSP-C and Pt/C before and after 1000-cycle cyclic voltammetry (CV) tests in 0.1 M KOH; d) Comparison of self-discharge rate of solid-state Zn-air batteries with Mo-N/C@MoS₂ and Pt/C; e) TEM image of Mo-N/C@MoS₂; f) Illustration of the preparation of NiCoS/Ti₃C₂T_x. Reprinted with permission from (a)^[92] Copyright 2016 American Chemical Society, (b), (c)^[93] Copyright 2017 WILEY-VCH Verlag GmbH & Co. KGaA, Weinheim, (d), (e)^[100] Copyright 2018 WILEY-VCH Verlag GmbH & Co. KGaA, Weinheim, (f)^[107] Copyright 2018 American Chemical Society.

carbonization of the precursor generates Co₄N, which is very different from other similar ZIF-67 carbonization processes that usually generate metal Co particles. The authors indicated that this could be associated with the nitrogenous gas atmosphere generated by the pyrolysis of ppy. The combination of Co₄N with high OER activity and Co–N–C with good ORR activity showed decent performance in rechargeable Zn–air batteries. Following Meng’s work, some other publication also reported the generation of transition metal nitrides (e.g., Fe₃N, FeN_x, CoN_x) or transition metal carbides (e.g., Fe₃C, Co₃C) from MOF precursors after high-temperature calcination.^[102–106] However, due to the complexity of the composition, further investigation into the role of these transition metal compounds on oxygen catalysis and on rechargeable Zn–air batteries is still required.

Co₂P particles encapsulated heteroatom-doped carbon matrix was developed using a self-template method (Figure 7b) by Ahn et al.^[93] Their work indicated that Co₂P mainly served as an active component for the OER, while N-doped carbon provided active sites for the ORR. Benefiting from the excellent bifunctional catalytic activities (Figure 7c), the catalyst demonstrated lower discharge and charge overpotential than commercial Pt/C for rechargeable Zn–air batteries. They suggested that Co₂P would be oxidized prior to the carbon materials in the Co₂P–carbon matrix, thus maintaining a highly efficient Co compound containing N-rich carbon matrix. Therefore, a remarkable cycling stability over 450 h was achieved. In a later report, Hao et al. demonstrate a Co and CoP embedded N-

doped carbon polyhedron.^[95] Similar to Ahn’s finding, Hao’s work also indicated that CoP would partially transform into CoO_x, which is beneficial to the catalytic OER activity and stability. When applied in a rechargeable Zn–air battery, the catalyst offered a small voltage gap during discharge–charge (0.78 V) in the initial cycle and the gap maintained at 0.96 V after 100 cycles.

A MoS₂ nanosheet wrapped N-doped carbon polyhedron (Mo-N-C@MoS₂) was proposed by Amiinu et al. (Figure 7e)^[100] The authors indicated that Mo atoms may have interacted with N atoms, the coupling of which optimized the electron distribution of N atoms, thus leading to improved oxygen adsorption which facilitated the ORR activity. In addition, MoS₂ may also enhance the accessibility of the active sites for reactants (O₂ and OH[−]), thereby providing better ionic diffusion. When used as a bifunctional catalyst in a rechargeable Zn–air battery, Mo-N-C@MoS₂ achieved a low discharge–charge voltage gap of 0.75 V. When further utilized in a solid-state Zn–air battery, a much-suppressed self-discharge rate was demonstrated (Figure 7d). Li et al. proposed a Co₉S₈ nanoparticles decorated N and S co-doped carbon via an elemental sulfur assisted calcination procedure.^[108] The catalyst demonstrated decent performance of both primary and rechargeable Zn–air batteries. Meng et al. reported a Co_{0.85}Se encapsulated N-doped carbon polyhedron by calcinating ZIF-67 precursor with the addition of elemental Se powder.^[96] The as-obtained material

also showed decent performance as a bifunctional air cathode in rechargeable Zn-air batteries.

MOF-derived transition metal compounds without a carbon support have also been reported. In a work proposed by Zou et al., ZIF-67 served as a precursor for forming Ni–Co LDH on the surface of $Ti_3C_2T_x$ Mxene (Figure 7f).^[107] The Ni–Co LDH was further converted into Ni–Co sulfide by heating at 400 °C under a CS_2 gas flow. After integrating $NiCoS/Ti_3C_2T_x$ with Pt/C, decent performance of rechargeable Zn-air batteries were achieved. In another work, amorphous Ni, Fe-based nanocubes with different heteroatoms (P, B, or S) were proposed by Xuan et al.^[109,110] After coupled with N-, S- doped carbon, the composites demonstrated similar performance as catalysts for rechargeable Zn-air batteries, which outperformed that with a Pt/C+Ir/C catalyst.

3.3. Metal-Free Carbons

Metal-free carbons represent another type of promising oxygen catalysts, especially for the ORR.^[33,111] While more investigations on their application in Zn-air batteries are still required, some pioneering works on this topic are valuable for guiding the further development. ZIF-8 with Zn metal node is the most studied precursor for synthesizing metal-free carbon materials, since the Zn intermediates produced are likely to evaporate during the high-temperature calcination process, thus leaving highly porous carbon frameworks with rich N dopants and ultrahigh specific surface areas.^[112]

In 2017, a carbon catalyst with photonic crystal structure was proposed by Yang et al.^[113] By using ZIF-8 as a carbon precursor and silica ordered arrays as a hard template, they obtained a highly ordered, macro-porous carbon catalyst with a

combination of highly catalytic N–C active centers and remarkable porosity (a_{BET} of 2546 m 2 g $^{-1}$, pore volume of 13.42 cm 3 g $^{-1}$). This feature provides excellent ORR performance for primary Zn-air batteries. Molten salt-assisted calcination has been shown to further optimize the morphology and porous structure.^[112,114,115] For example, Xuan et al. proposed a NaCl assisted production of N-doped, 3D hierarchically porous carbon from ZIF-8 precursor.^[115] The surface chemical states of nitrogen atoms from XPS analysis suggested that the NaCl molten salt plays an important role in tuning nitrogen coordination with carbon. Higher proportions of pyridinic-N and graphitic-N (N1 and N3, respectively, as shown in Figure 8a) were observed for the carbon catalyst with NaCl-assisted calcination. Due to the optimized N–C coordination and the unique morphological features, the primary Zn-air batteries demonstrated very high OCV of 1.54 V with no significant self-discharging (Figure 8b), good PPD of 207 mWcm $^{-2}$, and stable working performance over 200 h (Figure 8c).

Some other attempts have also been made for improving the OER performance of MOF-derived metal-free carbons by heteroatom doping such as nitrogen, boron, and phosphorus.^[116,117] Qian et al. obtained a N and B co-doped carbon by calcinating a Zn-containing MOF (MC-BIF-1 S).^[117] Unlike other N and B co-doped carbons synthesized from a post-treatment in N- and B-rich atmosphere, the material derived from the MOF demonstrated homogeneous dispersion of heteroatoms throughout the carbon matrix (Figure 8d). Compared with the mono-doped carbons derived from the N-containing precursor (ZIF-8) and the B-containing precursor (COF-5), the N and B dual doped carbon demonstrated better activity for the OER. This was associated with the promoted adsorption of hydroxyl ions and water molecules and also the improved charge transfer owing to the evenly dispersed N and

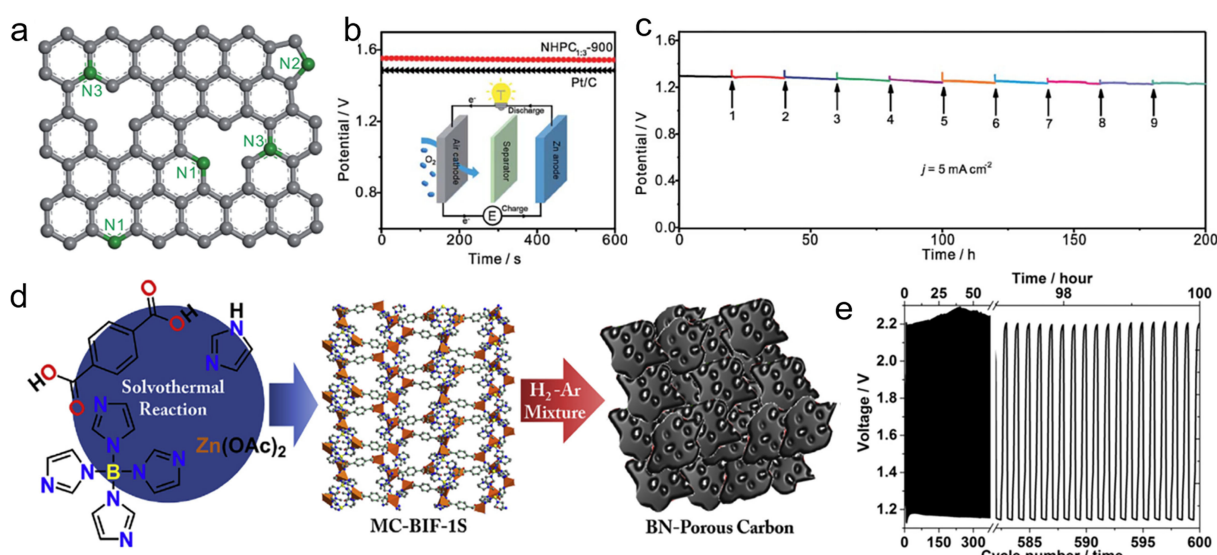


Figure 8. (a) Schematic structure of the N-doped hierarchical porous carbon (NHPC1:3-900), N1, N2 and N3 represent pyridinic-N, pyrrolic-N and graphitic-N, respectively. (b) comparison of OCV of primary Zn-air batteries with Pt/C and NHPC1:3-900-based ORR catalyst, (c) discharge stability of primary Zn-air batteries with NHPC1:3-900-based ORR catalyst. (d) The synthetic procedures of B- and N-doped carbon. (e) Cycling stability of a rechargeable Zn-air battery with B- and N-doped carbon as oxygen catalyst. Reprinted with permission from (a–c)^[115] Copyright 2018 Royal Society of Chemistry, (d,e)^[117] Copyright 2017 Elsevier.

B dopants around the positively charged C atoms. As a result, the catalyst demonstrated an acceptable charging potential of ~ 2.19 V at 2 mA cm^{-2} in a rechargeable Zn-air battery (Figure 8e), although this value is still inferior to that observed on MOF-derived metal compounds as oxygen catalysts. In a recent report, Li et al. designed N and P co-doped CNT clusters by calcination of a butyl methyl phosphonate (P containing organic precursor) modified ZIF-8,^[116] which delivered a charging potential of 2.1 V when applied as a bifunctional catalyst.

3.4. Optimization of MOF-Derived Catalysts

3.4.1. Morphology Design and Pore Tuning

The intention to design optimized morphologies for MOF-derived oxygen catalysts is mainly for improving kinetics of the

oxygen reactions by increasing the three-phase-boundaries (TPDs) among the catalyst, air (oxygen), and electrolyte.

In this regard, hollow and core/shell structures,^[43,60,84,105] 1D thin rods/bars,^[64,66,69,81,89,92,93,97,99,118-120] 2D thin sheets^[62,67,71,79,83,100,102,107] are shown to be favorable. In addition, highly interconnected 3D structures^[56,58,59,86,112-114] are also beneficial to improving the long-range electronic conductivity of the cathode.

To clarify the impact of morphologies on the activities of oxygen catalysis and Zn-air batteries, Li and coworkers reported a series of research results.^[60,89,99,121] For example, they designed a Co–N–C composite with a hollow structure by using a ZnO template for preparing the MOF precursor.^[60] During the calcination process, ZnO was reduced to Zn which was evaporated at a high temperature of 900°C in a N_2 flow. This left a large void within the resulting Co–N–C particle (Figure 9a). Compared to the Co–N–C polyhedron without a void

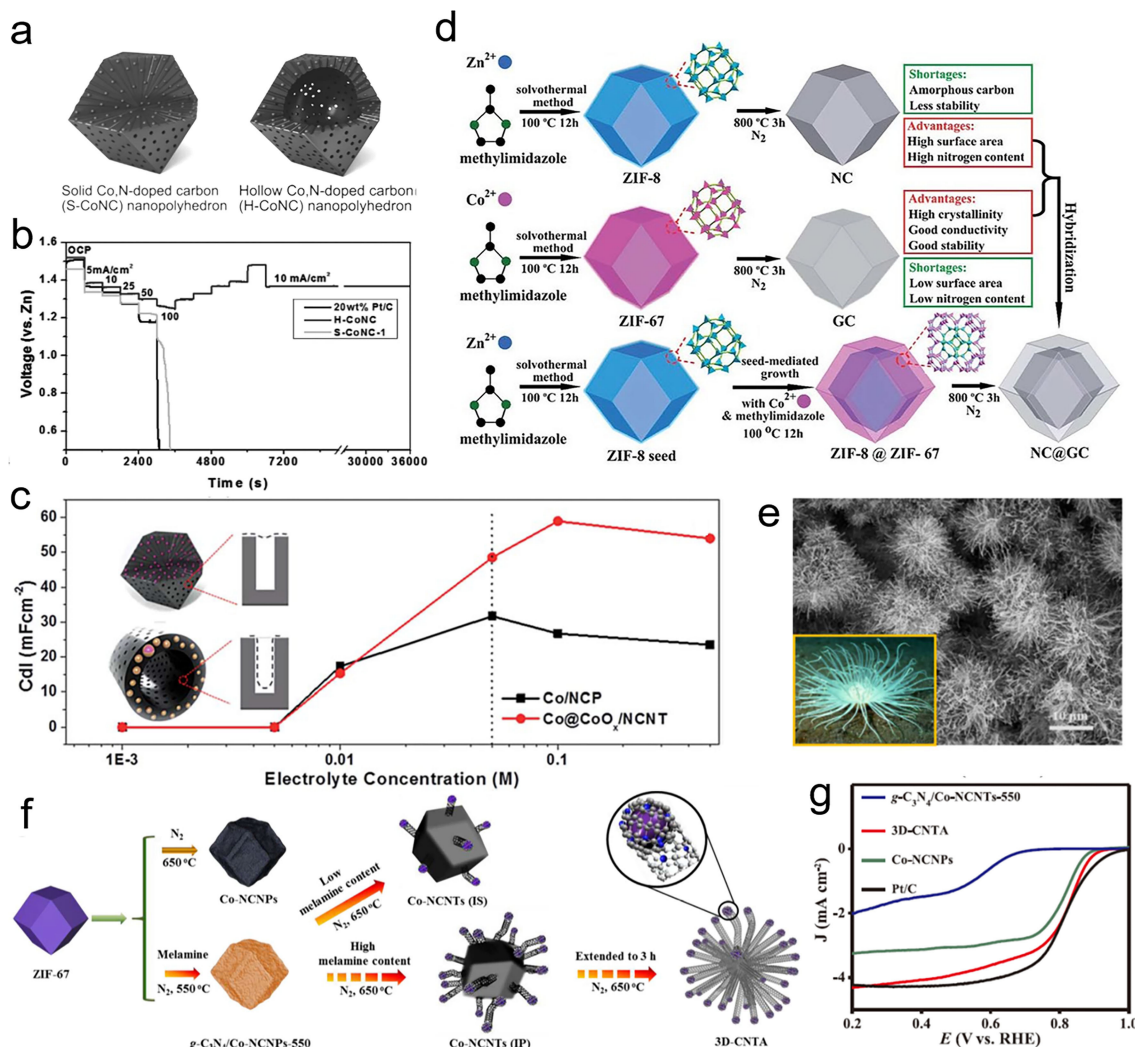


Figure 9. a) Illustration of the morphological differences between Co–N–C particle (S-CoNC) and hollow Co–N–C (H-CoNC), b) Comparison of the rate performances of S-CoNC, H-CoNC and Pt/C; c) Comparison of double-layer capacitance of Co–N–C composites with different morphologies; d) Typical synthetic procedures of ZIF-8 and ZIF-67 derived carbon-based materials and their characteristics; e) SEM image of 3D-CNTA, inset shows a digital photo of an actiniae, f) Illustration of the synthetic procedures of 3D-CNTA and Co-NCNTs, g) Voltammograms comparison of 3D-CNTA, Co-NCNTs and Pt/C. Reprinted with permission from (a), (b)^[60] Copyright 2017 WILEY-VCH Verlag GmbH & Co. KGaA, Weinheim, (c)^[89] Copyright 2017 Royal Society of Chemistry, (d)^[112] Copyright 2015 American Chemical Society, (e)–(g)^[56] Copyright 2017 Elsevier.

(Figure 9a), the hollow material demonstrated a dramatic improvement of high-rate performance for primary Zn-air batteries (Figure 9b). As proved by KSCN poisoning and CV measurements, much improved electrochemical accessibility of the oxygen was demonstrated for the Co–N–C material with the hollow structure. In addition, the hollow structure presented an additional confinement effect of oxygen, especially in a highly concentrated KOH solution (e.g., 6 M). These features facilitated the kinetics of the ORR, thereby achieving better Zn-air battery performance. In another example, Co and CoO_x encapsulated 1D CNTs were prepared using a ZnO-assisted calcination.^[89] As demonstrated in Figure 6d, the rate-performance for a Zn-air battery with the Co@CoO_x material with a 1D hollow nanotube morphology was much superior to that with the Co/NCP material with a conventional morphology of a polyhedron. This could be associated with the improved electrochemical accessibility of the reactant resulting from the 1D CNT morphology. As indicated in Figure 9c, the material with a tubular morphology shows much higher electrochemically active surface areas in alkaline solution.

Besides the above-mentioned ZnO-assisted synthesis,^[60,89,99,116] hard-templated synthesis with other templates such as SiO_2 ,^[113] MnO_2 ,^[97] and metal Te^[69] have also been reported. In addition, other methods like hydrothermal^[119] and electrospinning^[81,118] have also been developed to synthesize MOFs with special morphologies. The resulting catalysts demonstrated a significant improvement in the performance of Zn-air batteries. The porosity of MOF derivatives also plays an important role in the performance via optimizing mass transport on the air cathode. It is worth mentioning that the type of MOF precursors has a fundamental effect on the porosity of the resulting carbon-based materials. Tang et al. found that carbons from a ZIF-8 precursor possess higher surface areas than those from ZIF-67 (Figure 9d).^[112] Most of the a_{BET} data in Tables S1 and S2 also support this observation. The higher surface area of ZIF-8 could be partially ascribed to the poor capability of Zn for carbon reforming at high temperatures, which produced a highly porous, amorphous carbon structure. In addition, the Zn node in the MOF precursor would be easily evaporated during the calcination, leaving abundant pores in the resulting carbon.^[61] A strategy that couples ZIF-8 with ZIF-67 at a morphological or compositional scale has been applied to tune the porosity of the target catalysts.^[43,60–62,123] Other methods for manipulating the porosity of MOF-derived materials such as hard-templated synthesis^[60,89,99,113,116] and molten salt assisted synthesis^[79,112,114,115] have also been reported.

3.4.2. Electronic Conductivity Improvement

To ensure smooth electron transfer throughout the air cathode for batteries operating at high current rates, efforts have been made to integrate highly graphitized carbon into the MOF-derived catalysts. In situ growing MOF precursor on highly conductive carbons such as carbon black, carbon cloths^[92], carbon fibers,^[81] CNTs^[58] and carbon nanohorns^[61] is a facile strategy to get a long-range interconnected conductive frame-

work throughout the active sites. Liu et al. proposed another strategy to obtain graphene frameworks by exfoliation of carbon fibers.^[62] The exfoliated carbon offered a highly electronic conductive 2D surface for the *in situ* growth of MOF. The resulting Co–N–C on graphene catalyst demonstrated better PPD for primary Zn-air batteries than the Co–N–C on carbon paper catalyst by a physical drop-casting method.

Owing to the high carbon reforming capability of transition metal particles under a carbonaceous atmosphere at high temperatures (usually $>600^\circ\text{C}$), spontaneously growing CNTs on a MOF-derived carbon-based material is another promising strategy.^[43,55,56,59,94,95,98] For example, Wang et al. utilized melamine as a N-rich precursor for improving the Co catalyzed growth of CNTs (Figure 9f).^[56] They indicated that a high concentration of melamine facilitated the CNT growing process. A prolonged duration of the growing process produced an actinia morphology (Figure 9e), which demonstrated improved ORR activity (Figure 9g) and decent performance of Zn-air batteries. It is also noted that different metals may have distinguished catalytic efficiencies for the CNT formation.^[99] In a previous report, Fe demonstrated a CNT formation rate that doubles that of Co.^[124] Therefore, the catalytic growth of CNTs should be rationally designed (in terms of duration time, temperature, composition of the precursors) to prevent the collapse of the morphologies of MOF precursors and the dramatic decrease of surface areas.^[54]

4. Conclusion and Perspectives

In this review, the recent development of MOF-derived catalysts for primary and rechargeable Zn-air batteries is summarized. Transition metal–nitrogen–carbon (TM–N–C) composites, carbon-based transition metal compounds, and metal-free carbons have been synthesized via thermal carbonization of the rationally designed MOF precursors. As illustrated in Figure 2 and indicated in Tables S1 and S2, the MOF-derived materials usually inherit the morphologies of the MOF precursors and have highly porous structure, which can provide abundant active surface for the oxygen reactions (ORR and OER). In aqueous electrolyte-based rechargeable Zn-air batteries, catalysts with high ORR activity are vital for decreasing the discharging overpotential while those with high OER activity is beneficial to decreasing the charging overpotential. Among the many reported MOF derivatives, TM–N–C composites demonstrate extraordinary ORR activity due to the uniformly dispersed TM–N_x active sites. TM–N–C with single-atom TM show further improvement in the ORR activity. MOF-derived carbon-based transition metal compounds present excellent bifunctional catalysis for ORR and OER. Furthermore, MOF-derived metal-free carbons are another family of potential catalyst for use as the air cathode of Zn-air batteries. Further optimization of the morphologies, porous structures, and electronic conductivities of the MOF-derived materials is also important for promoting the performance of the batteries, especially at high current densities. MOF-derived catalysts with morphologies like hollow and core/shell structures, 1D thin rods/bars, 2D thin sheets and

complex 3D architectures have been developed. Pore tuning of the catalyst can be achieved by adopting different MOF-precursors, hard templates, or molten salts. Long-range electronic conductivity can be improved by integrating highly conductive carbons via coupling MOF precursors with carbons or via *in-situ* spontaneous growth of CNTs catalyzed by transition metal particles.

Despite the progress achieved thus far, as illustrated in Figure 10, challenges still remain in an effort to developing highly efficient Zn-air battery systems based on MOF-based catalysts.

First of all, even though the activities toward the ORR and OER processes have a fundamental impact on the performance of Zn-air batteries, other issues like the selectivity of the oxygen reduction process and the oxygen diffusion from the ambient atmosphere to the reactive three-phase-boundary should also be given enough attention for the development of new MOF-derived catalysts or air cathodes in the future (Figure 10a). For example, in Zn-air batteries, the two-electron process not only reduces energy conversion efficiency but also leads to inevitable side reactions between the produced superoxide and the Zn anode, causing self-discharge of the batteries.^[112] Even though the number of electrons transferred in the ORR for most reported MOF-derived catalysts is close to 4, indicating good suppression of superoxide generation, the long-term accumulation impact on the battery performance should also be considered. Another concern is that the widely used 6 M KOH electrolyte in Zn-air batteries are far more concentrated than those in the experimental systems for the evaluation of ORR and OER (e.g., 0.1 M or 1 M KOH). In the highly concentrated KOH, the solubility of oxygen is several times lower.^[60] Improvement of oxygen diffusion via a surface or architecture engineering (e.g., optimization of surface wettability and ordering of the porous structure) on the air cathode is seldomly reported in the

works about MOF-derived catalysts, which would be valuable for further investigation.

Secondly, the use of pristine MOFs as oxygen catalysts would be an attractive topic for further study (Figure 10b). A wide range of MOF materials themselves show remarkable TM-Nx coordination at an atomic scale. In addition, the well-defined ordered pore structure with extremely high specific surface area also promises the direct utilization of MOFs as ORR and OER catalysts for Zn-air batteries. In recent years, some pioneering works have reported the possibility of utilizing MOFs as oxygen catalysts.^[125] For example, Zhang and co-workers reported a novel Co-containing porphyrin covalent organic framework (COF) for aqueous and flexible Zn-air batteries which demonstrated high PPD as well as durable cycling life over 200 cycles.^[126] Another very recent work proposed by Chen et al. presented decent rechargeable performance of Zn-air batteries with a Co-MOF decorated graphite foam as a bifunctional oxygen catalyst.^[127] These works may stimulate more exciting investigations into MOFs and COFs for Zn-air batteries.

Furthermore, as presented in Tables 1 and 2, performances of the Zn-air batteries were usually evaluated at a relatively low current density of less than 25 mA cm⁻². To achieve a higher power density for practical utilization, the rational design of new catalysts and battery configurations which can afford high-rate (higher than 10 mA cm⁻²) discharge and charge is required (Figure 10c). Efforts should also be made to address the side reactions (e.g., decomposition of electrolyte, degradation of the oxygen catalysts, and passivation of the Zn surface) involved in high-rate performing aqueous Zn-air batteries.

Lastly, some works mentioned in this review have also utilized MOF-derived catalysts in flexible^[59,75,83,92,94,128] or rigid^[62,65,66,74,80,97,100] solid-state Zn-air batteries. These works present a promising application for portable and wearable

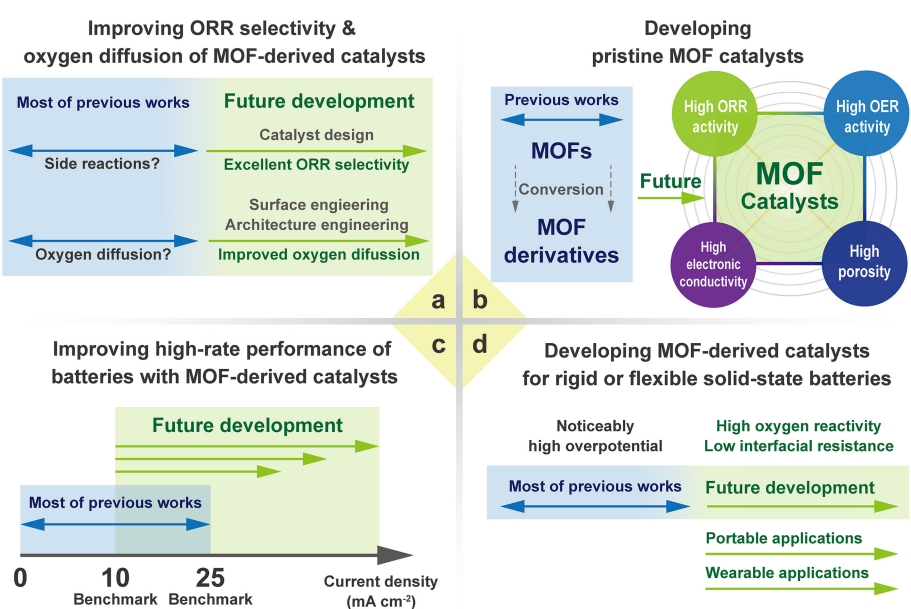


Figure 10. Schematic illustration of challenges and promising prospects toward future development of MOF-based and MOF-derived catalysts for high-performance Zn-air batteries.

devices. However, most of these batteries suffer from a more noticeable overpotential than the conventional aqueous systems. Advanced designs of solid-state batteries with both high oxygen reactivities and low interfacial resistances are required (Figure 10d).^[40]

Zn-air battery is a mature energy storage system for its long history of commercialization. At the same time, newly-emerged fundamental investigations (e.g., highly efficient oxygen catalyst) and techniques (e.g., wearable devices) have also made Zn-air battery a promising research field which has been receiving increasing interests worldwide. Further development of functional MOFs and MOF-derived catalysts would provide better solutions to the issues outlined above. More exiting research results for tackling the challenges of Zn-air batteries are expected in the recent future.

Acknowledgements

The authors would like to thank the Australia Research Council for supporting the project under contract DP150104365 and DP160104835.

Conflict of Interest

The authors declare no conflict of interest.

Keywords: electrocatalysis • metal-organic frameworks • oxygen reduction reaction • oxygen evolution reaction • zinc-air battery

- [1] M. Winter, R. J. Brodd, *Chem. Rev.* **2004**, *104*, 4245–4270.
- [2] F. Wang, X. Wu, C. Li, Y. Zhu, L. Fu, Y. Wu, X. Liu, *Energy Environ. Sci.* **2016**, *9*, 3570–3611.
- [3] Z. Yang, J. Zhang, M. C. W. Kintner-Meyer, X. Lu, D. Choi, J. P. Lemmon, J. Liu, *Chem. Rev.* **2011**, *111*, 3577–3613.
- [4] a) F. Cheng, J. Chen, *Chem. Soc. Rev.* **2012**, *41*, 2172–2192; b) L. Li, Z.-w. Chang, X.-B. Zhang, *Adv. Sustainable Syst.* **2017**, *1*, 1700036; c) D. Geng, N. Ding, T. S. A. Hor, S. W. Chien, Z. Liu, D. Wuu, X. Sun, Y. Zong, *Adv. Energy Mater.* **2016**, *6*, 1502164.
- [5] a) D. Aurbach, B. D. McCloskey, L. F. Nazar, P. G. Bruce, *Nat. Energy* **2016**, *1*, 16128; b) M.-K. Song, S. Park, F. M. Alamgir, J. Cho, M. Liu, *Mater. Sci. Eng. R* **2011**, *72*, 203–252.
- [6] a) Y. Li, J. Lu, *ACS Energy Lett.* **2017**, *2*, 1370–1377; b) M. A. Rahman, X. Wang, C. Wen, *J. Electrochem. Soc.* **2013**, *160*, A1759–A1771.
- [7] A. C. Luntz, B. D. McCloskey, *Chem. Rev.* **2014**, *114*, 11721–11750.
- [8] Y. Li, H. Dai, *Chem. Soc. Rev.* **2014**, *43*, 5257–5275.
- [9] X. Han, X. Li, J. White, C. Zhong, Y. Deng, W. Hu, T. Ma, *Adv. Energy Mater.* **2018**, *8*, 1801396.
- [10] Y. Liu, P. He, H. Zhou, *Adv. Energy Mater.* **2018**, *8*, 1701602.
- [11] N. Imanishi, O. Yamamoto, *Mater. Today* **2014**, *17*, 24–30.
- [12] a) K. Liao, S. Wu, X. Mu, Q. Lu, M. Han, P. He, Z. Shao, H. Zhou, *Adv. Mater.* **2018**, *30*, 1705711; b) X. Zou, Q. Lu, Y. Zhong, K. Liao, W. Zhou, Z. Shao, *Small* **2018**, *14*, 1801798.
- [13] Z.-L. Wang, D. Xu, J.-J. Xu, X.-B. Zhang, *Chem. Soc. Rev.* **2014**, *43*, 7746–7786.
- [14] J. Fu, Z. P. Cano, M. G. Park, A. Yu, M. Fowler, Z. Chen, *Adv. Mater.* **2017**, *29*, 1604685.
- [15] D. U. Lee, P. Xu, Z. P. Cano, A. G. Kashkooli, M. G. Park, Z. Chen, *J. Mater. Chem. A* **2016**, *4*, 7107–7134.
- [16] F.-L. Meng, K.-H. Liu, Y. Zhang, M.-M. Shi, X.-B. Zhang, J.-M. Yan, Q. Jiang, *Small* **2018**, *14*, 1703843.
- [17] J. Zhang, Z. Zhao, Z. Xia, L. Dai, *Nat. Nanotechnol.* **2015**, *10*, 444–452.
- [18] H.-F. Wang, C. Tang, B. Wang, B.-Q. Li, Q. Zhang, *Adv. Mater.* **2017**, *29*, 1702327.
- [19] J. Pan, Y. Y. Xu, H. Yang, Z. Dong, H. Liu, B. Y. Xia, *Adv. Sci.* **2018**, *5*, 1700691.
- [20] X. Cai, L. Lai, J. Lin, Z. Shen, *Mater. Horiz.* **2017**, *4*, 945–976.
- [21] a) M. Tahir, L. Pan, F. Idrees, X. Zhang, L. Wang, J.-J. Zou, Z. L. Wang, *Nano Energy* **2017**, *37*, 136–157; b) W. Xia, A. Mahmood, Z. Liang, R. Zou, S. Guo, *Angew. Chem. Int. Ed.* **2016**, *55*, 2650–2676; *Angew. Chem.* **2016**, *128*, 2698–2726.
- [22] M. Shao, Q. Chang, J.-P. Dodelet, R. Chenitz, *Chem. Rev.* **2016**, *116*, 3594–3657.
- [23] a) Y. Qian, I. A. Khan, D. Zhao, *Small* **2017**, *13*, 1701143; b) E. Davari, D. G. Ivey, *Sustainable Energy Fuels* **2018**, *2*, 39–67.
- [24] W. T. Hong, M. Risch, K. A. Stoerzinger, A. Grimaud, J. Suntivich, Y. Shao-Horn, *Energy Environ. Sci.* **2015**, *8*, 1404–1427.
- [25] a) J. Yu, G. Chen, J. Sunarso, Y. Zhu, R. Ran, Z. Zhu, W. Zhou, Z. Shao, *Adv. Sci.* **2016**, *3*, 1600060; b) L. Xu, Q. Jiang, Z. Xiao, X. Li, J. Huo, S. Wang, L. Dai, *Angew. Chem. Int. Ed.* **2016**, *55*, 5277–5281; *Angew. Chem.* **2016**, *128*, 5363–5367; c) P. Tan, B. Chen, H. Xu, W. Cai, W. He, M. Liu, Z. Shao, M. Ni, *Small* **2018**, *14*, 1800225.
- [26] Y. Zhu, W. Zhou, Y. Chen, J. Yu, M. Liu, Z. Shao, *Adv. Mater.* **2015**, *27*, 7150–7155.
- [27] a) H. Yin, Z. Tang, *Chem. Soc. Rev.* **2016**, *45*, 4873–4891; b) H. Liang, F. Meng, M. Cabán-Acevedo, L. Li, A. Forticaux, L. Xiu, Z. Wang, S. Jin, *Nano Lett.* **2015**, *15*, 1421–1427; c) Z. Lu, W. Xu, W. Zhu, Q. Yang, X. Lei, J. Liu, Y. Li, X. Sun, X. Duan, *Chem. Commun.* **2014**, *50*, 6479–6482.
- [28] a) D. Chen, C. Chen, Z. M. Baiyee, Z. Shao, F. Ciucci, *Chem. Rev.* **2015**, *115*, 9869–9921; b) X. Xu, W. Wang, W. Zhou, Z. Shao, *Small Methods* **2018**, *2*, 1800071; c) Y. Zhu, W. Zhou, Z. Shao, *Small* **2017**, *13*, 1603793; d) X. Xu, C. Su, W. Zhou, Y. Zhu, Y. Chen, Z. Shao, *Adv. Sci.* **2016**, *3*, 1500187; e) G. Chen, W. Zhou, D. Guan, J. Sunarso, Y. Zhu, X. Hu, W. Zhang, Z. Shao, *Sci. Adv.* **2017**, *3*, e1603206; f) Y. Zhu, W. Zhou, Y. Zhong, Y. Bu, X. Chen, Q. Zhong, M. Liu, Z. Shao, *Adv. Energy Mater.* **2017**, *7*, 1602122; g) X. Xu, Y. Chen, W. Zhou, Y. Zhong, D. Guan, Z. Shao, *Adv. Mater. Interfaces* **2018**, *5*, 1701693.
- [29] a) H. Hu, L. Han, M. Yu, Z. Wang, X. W. Lou, *Energy Environ. Sci.* **2016**, *9*, 107–111; b) Q. Liu, J. Jin, J. Zhang, *ACS Appl. Mater. Interfaces* **2013**, *5*, 5002–5008; c) W. Zhou, X.-J. Wu, X. Cao, X. Huang, C. Tan, J. Tian, H. Liu, J. Wang, H. Zhang, *Energy Environ. Sci.* **2013**, *6*, 2921–2924.
- [30] a) X. L. Tian, L. Wang, B. Chi, Y. Xu, S. Zaman, K. Qi, H. Liu, S. Liao, B. Y. Xia, *ACS Catal.* **2018**, *8*, 8970–8975; b) K. Xu, P. Chen, X. Li, Y. Tong, H. Ding, X. Wu, W. Chu, Z. Peng, C. Wu, Y. Xie, *J. Am. Chem. Soc.* **2015**, *137*, 4119–4125; c) P. Chen, K. Xu, Z. Fang, Y. Tong, J. Wu, X. Lu, X. Peng, H. Ding, C. Wu, Y. Xie, *Angew. Chem. Int. Ed.* **2015**, *54*, 14710–14714; *Angew. Chem.* **2015**, *127*, 14923–14927; d) C. Guan, A. Sumboja, W. Zang, Y. Qian, H. Zhang, X. Liu, Z. Liu, D. Zhao, S. J. Pennycook, J. Wang, *Energy Storage Mater.* **2019**, *16*, 243–250.
- [31] a) P. He, X.-Y. Yu, X. W. Lou, *Angew. Chem. Int. Ed.* **2017**, *56*, 3897–3900; *Angew. Chem.* **2017**, *129*, 3955–3958; b) X.-Y. Yu, Y. Feng, B. Guan, X. W. Lou, U. Paik, *Energy Environ. Sci.* **2016**, *9*, 1246–1250; c) Y.-P. Zhu, Y.-P. Liu, T.-Z. Ren, Z.-Y. Yuan, *Adv. Funct. Mater.* **2015**, *25*, 7337–7347; d) L.-A. Stern, L. Feng, F. Song, X. Hu, *Energy Environ. Sci.* **2015**, *8*, 2347–2351.
- [32] a) T. Y. Ma, J. L. Cao, M. Jaroniec, S. Z. Qiao, *Angew. Chem. Int. Ed.* **2016**, *55*, 1138–1142; *Angew. Chem.* **2016**, *128*, 1150–1154; b) L. Zhao, B. Dong, S. Li, L. Zhou, L. Lai, Z. Wang, S. Zhao, M. Han, K. Gao, M. Lu, X. Xie, B. Chen, Z. Liu, X. Wang, H. Zhang, H. Li, J. Liu, H. Zhang, X. Huang, W. Huang, *ACS Nano* **2017**, *11*, 5800–5807; c) J.-S. Li, S.-L. Li, Y.-J. Tang, M. Han, Z.-H. Dai, J.-C. Bao, Y.-Q. Lan, *Chem. Commun.* **2015**, *51*, 2710–2713; d) B. Y. Guan, L. Yu, X. W. Lou, *Energy Environ. Sci.* **2016**, *9*, 3092–3096.
- [33] H. B. Yang, J. Miao, S.-F. Hung, J. Chen, H. B. Tao, X. Wang, L. Zhang, R. Chen, J. Gao, H. M. Chen, L. Dai, B. Liu, *Sci. Adv.* **2016**, *2*, e1501122.
- [34] D.-W. Wang, D. Su, *Energy Environ. Sci.* **2014**, *7*, 576–591.
- [35] a) H. Furukawa, K. E. Cordova, M. O'Keeffe, O. M. Yaghi, *Science* **2013**, *341*, 1230444; b) A. Morozan, F. Jaouen, *Energy Environ. Sci.* **2012**, *5*, 9269–9290; c) F.-Y. Yi, R. Zhang, H. Wang, L.-F. Chen, L. Han, H.-L. Jiang, Q. Xu, *Small Methods* **2017**, *1*, 1700187.
- [36] a) W. Xia, A. Mahmood, R. Zou, Q. Xu, *Energy Environ. Sci.* **2015**, *8*, 1837–1866; b) Y. Liu, Z. Wang, Y. Zhong, M. Tade, W. Zhou, Z. Shao, *Adv. Funct. Mater.* **2017**, *27*, 1701229; c) H. B. Wu, X. W. Lou, *Sci. Adv.* **2017**, *3*, eaap9252; d) B. Y. Guan, X. Y. Yu, H. B. Wu, X. W. Lou, *Adv. Mater.* **2017**, *29*, 1703614; e) Y. Zhong, X. Xu, Y. Liu, W. Wang, Z. Shao, *Polyhedron* **2018**, *155*, 464–484.

- [37] a) W. Wang, X. Xu, W. Zhou, Z. Shao, *Adv. Sci.* **2017**, *4*, 1600371; b) Y. Zhu, G. Chen, X. Xu, G. Yang, M. Liu, Z. Shao, *ACS Catal.* **2017**, *7*, 3540–3547; c) B. Y. Guan, L. Yu, X. W. Lou, *Adv. Sci.* **2017**, *4*, 1700247; d) C.-H. Su, C.-W. Kung, T.-H. Chang, H.-C. Lu, K.-C. Ho, Y.-C. Liao, *J. Mater. Chem. A* **2016**, *4*, 11094–11102; e) J. Nai, Y. Lu, L. Yu, X. Wang, W. Lou, *Adv. Mater.* **2017**, *29*, 1703870; f) Y.-Z. Chen, R. Zhang, L. Jiao, H.-L. Jiang, *Coord. Chem. Rev.* **2018**, *362*, 1–23; g) Q. Ren, H. Wang, X.-F. Lu, Y.-X. Tong, G.-R. Li, *Adv. Sci.* **2018**, *5*, 1700515; h) L. Yang, X. Zeng, W. Wang, D. Cao, *Adv. Funct. Mater.* **2018**, *28*, 1704537; i) S.-N. Zhao, X.-Z. Song, S.-Y. Song, H.-j. Zhang, *Coord. Chem. Rev.* **2017**, *337*, 80–96; j) N. Kornienko, Y. Zhao, C. S. Kley, C. Zhu, D. Kim, S. Lin, C. J. Chang, O. M. Yaghi, P. Yang, *J. Am. Chem. Soc.* **2015**, *137*, 14129–14135.
- [38] a) H. Zhang, H. Osgood, X. Xie, Y. Shao, G. Wu, *Nano Energy* **2017**, *31*, 331–350; b) J. Liu, D. Zhu, C. Guo, A. Vasileff, S.-Z. Qiao, *Adv. Energy Mater.* **2017**, *7*, 1700518; c) N. Cheng, L. Ren, X. Xu, Y. Du, S. X. Dou, *Adv. Energy Mater.* **2018**, *8*, 1801257.
- [39] a) H.-F. Wang, C. Tang, Q. Zhang, *Adv. Funct. Mater.* **2018**, 1803329, in press, DOI: 10.1002/adfm.201803329; b) A. R. Mainar, E. Iruin, L. C. Colmenares, A. Kvasha, I. de Meatza, M. Bengoechea, O. Leonet, I. Boyano, Z. Zhang, J. Alberto Blazquez, *J. Energy Storage* **2018**, *15*, 304–328; c) P. Pei, K. Wang, Z. Ma, *Appl. Energy* **2014**, *128*, 315–324.
- [40] P. Tan, B. Chen, H. Xu, H. Zhang, W. Cai, M. Ni, M. Liu, Z. Shao, *Energy Environ. Sci.* **2017**, *10*, 2056–2080.
- [41] M. Xu, D. G. Ivey, Z. Xie, W. Qu, *J. Power Sources* **2015**, *283*, 358–371.
- [42] a) X. Li, S. Zheng, L. Jin, Y. Li, P. Geng, H. Xue, H. Pang, Q. Xu, *Adv. Energy Mater.* **2018**, *8*, 1800716; b) H. Tang, M. Zheng, Q. Hu, Y. Chi, B. Xu, S. Zhang, H. Xue, H. Pang, *J. Mater. Chem. A* **2018**, *6*, 13999–14024; c) T. Yu, J. Fu, R. Cai, A. Yu, Z. Chen, *IEEE Nanotechnol. Mag.* **2017**, *11*, 29–55; d) G. Fu, Y. Tang, J.-M. Lee, *ChemElectroChem* **2018**, *5*, 1424–1434.
- [43] Z. Wang, Y. Lu, Y. Yan, T. Y. P. Larissa, X. Zhang, D. Wuu, H. Zhang, Y. Yang, X. Wang, *Nano Energy* **2016**, *30*, 368–378.
- [44] P. Sapkota, H. Kim, *J. Ind. Eng. Chem.* **2009**, *15*, 445–450.
- [45] a) D. Yang, L. Zhang, X. Yan, X. Yao, *Small Methods* **2017**, *1*, 1700209; b) R. Cao, J.-S. Lee, M. Liu, J. Cho, *Adv. Energy Mater.* **2012**, *2*, 816–829.
- [46] D. B. Sepa, M. V. Vojnovic, A. Damjanovic, *Electrochim. Acta* **1981**, *26*, 781–793.
- [47] J. K. Nørskov, J. Rossmeisl, A. Logadottir, L. Lindqvist, J. R. Kitchin, T. Bligaard, H. Jónsson, *J. Phys. Chem. B* **2004**, *108*, 17886–17892.
- [48] Y. Zheng, Y. Jiao, Y. Zhu, Q. Cai, A. Vasileff, L. H. Li, Y. Han, Y. Chen, S.-Z. Qiao, *J. Am. Chem. Soc.* **2017**, *139*, 3336–3339.
- [49] J. Suntivich, H. A. Gasteiger, N. Yabuuchi, H. Nakanishi, J. B. Goodenough, Y. Shao-Horn, *Nat. Chem.* **2011**, *3*, 546–550.
- [50] Y. Jiao, Y. Zheng, M. Jaroniec, S. Z. Qiao, *Chem. Soc. Rev.* **2015**, *44*, 2060–2086.
- [51] a) J. Rossmeisl, A. Logadottir, J. K. Nørskov, *Chem. Phys.* **2005**, *319*, 178–184; b) J. Rossmeisl, Z.-W. Qu, H. Zhu, G.-J. Kroes, J. K. Nørskov, *J. Electroanal. Chem.* **2007**, *607*, 83–89.
- [52] I. C. Man, H.-Y. Su, F. Calle-Vallejo, H. A. Hansen, J. I. Martínez, N. G. Inoglu, J. Kitchin, T. F. Jaramillo, J. K. Nørskov, J. Rossmeisl, *ChemCatChem* **2011**, *3*, 1159–1165.
- [53] B. Y. Xia, Y. Yan, N. Li, H. B. Wu, X. W. Lou, X. Wang, *Nat. Energy* **2016**, *1*, 15006.
- [54] E. Zhang, Y. Xie, S. Ci, J. Jia, P. Cai, L. Yi, Z. Wen, *J. Mater. Chem. A* **2016**, *4*, 17288–17298.
- [55] S. Dou, X. Li, L. Tao, J. Huo, S. Wang, *Chem. Commun.* **2016**, *52*, 9727–9730.
- [56] S. Wang, J. Qin, T. Meng, M. Cao, *Nano Energy* **2017**, *39*, 626–638.
- [57] J.-C. Li, X.-T. Wu, L.-J. Chen, N. Li, Z.-Q. Liu, *Energy* **2018**, *156*, 95–102.
- [58] H. B. Aiyappa, S. N. Bhange, V. P. Sivasankaran, S. Kurungot, *ChemElectroChem* **2017**, *4*, 2928–2933.
- [59] Z. Li, M. Shao, Q. Yang, Y. Tang, M. Wei, D. G. Evans, X. Duan, *Nano Energy* **2017**, *37*, 98–107.
- [60] X. Song, L. Guo, X. Liao, J. Liu, J. Sun, X. Li, *Small* **2017**, *13*, 1700238.
- [61] J. Zhang, C. Wu, M. Huang, Y. Zhao, J. Li, L. Guan, *ChemCatChem* **2018**, *10*, 1336–1343.
- [62] S. Liu, M. Wang, X. Sun, N. Xu, J. Liu, Y. Wang, T. Qian, C. Yan, *Adv. Mater.* **2018**, *30*, 1704898.
- [63] M. Zeng, Y. Liu, F. Zhao, K. Nie, N. Han, X. Wang, W. Huang, X. Song, J. Zhong, Y. Li, *Adv. Funct. Mater.* **2016**, *26*, 4397–4404.
- [64] M. Zhang, Q. Dai, H. Zheng, M. Chen, L. Dai, *Adv. Mater.* **2018**, *30*, 1705431.
- [65] T. Wang, Z. Kou, S. Mu, J. Liu, D. He, I. S. Amiinu, W. Meng, K. Zhou, Z. Luo, S. Chaemchuen, F. Verpoort, *Adv. Funct. Mater.* **2018**, *28*, 1705048.
- [66] I. S. Amiinu, X. Liu, Z. Pu, W. Li, Q. Li, J. Zhang, H. Tang, H. Zhang, S. Mu, *Adv. Funct. Mater.* **2018**, *28*, 1704638.
- [67] L. Gao, S. Chen, R. Cai, Q. Zhao, X. Zhao, D. Yang, *Global Challenges* **2018**, *2*, 1700086.
- [68] K. Kim, K. J. Lopez, H.-J. Sun, J.-C. An, G. Park, J. Shim, *J. Appl. Electrochem.* **2018**, *48*, 1231–1241.
- [69] S. H. Ahn, X. Yu, A. Manthiram, *Adv. Mater.* **2017**, *29*, 1606534.
- [70] W. Wei, X. Shi, P. Gao, S. Wang, W. Hu, X. Zhao, Y. Ni, X. Xu, Y. Xu, W. Yan, H. Ji, M. Cao, *Nano Energy* **2018**, *52*, 29–37.
- [71] J. Zhu, M. Xiao, Y. Zhang, Z. Jin, Z. Peng, C. Liu, S. Chen, J. Ge, W. Xing, *ACS Catal.* **2016**, *6*, 6335–6342.
- [72] B. Y. Guan, Y. Lu, Y. Wang, M. Wu, X. W. Lou, *Adv. Funct. Mater.* **2018**, *28*, 1706738.
- [73] Z. Liu, J. Liu, H. B. Wu, G. Shen, Z. Le, G. Chen, Y. Lu, *Nanoscale* **2018**, *10*, 16996–17001.
- [74] H. Jin, H. Zhou, W. Li, Z. Wang, J. Yang, Y. Xiong, D. He, L. Chen, S. Mu, *J. Mater. Chem. A* **2018**, in press, DOI: 10.1039/c8ta07849a.
- [75] L. Ma, S. Chen, Z. Pei, Y. Huang, G. Liang, F. Mo, Q. Yang, J. Su, Y. Gao, J. A. Zapien, C. Zhi, *ACS Nano* **2018**, *12*, 1949–1958.
- [76] Q. Lai, J. Zhu, Y. Zhao, Y. Liang, J. He, J. Chen, *Small* **2017**, *13*, 1700740.
- [77] J. He, T. Gao, T. Jiang, B. Mu, Y. Suo, Z. Zhang, J. Su, *ChemistrySelect* **2018**, *3*, 7913–7920.
- [78] P. Cai, S. Ci, E. Zhang, P. Shao, C. Cao, Z. Wen, *Electrochim. Acta* **2016**, *220*, 354–362.
- [79] W. Niu, Y. Yang, *ACS Appl. Energy Mater.* **2018**, *1*, 2440–2445.
- [80] Z. Wang, H. Jin, T. Meng, K. Liao, W. Meng, J. Yang, D. He, Y. Xiong, S. Mu, *Adv. Funct. Mater.* **2018**, *1802596*.
- [81] Y. Zhao, Q. Lai, J. Zhu, J. Zhong, Z. Tang, Y. Luo, Y. Liang, *Small* **2018**, *14*, 1704207.
- [82] a) Y. Chen, S. Ji, C. Chen, Q. Peng, D. Wang, Y. Li, *Joule* **2018**, *2*, 1242–1264; b) P. Yin, T. Yao, Y. Wu, L. Zheng, Y. Lin, W. Liu, H. Ju, J. Zhu, X. Hong, Z. Deng, G. Zhou, S. Wei, Y. Li, *Angew. Chem. Int. Ed.* **2016**, *55*, 10800–10805; *Angew. Chem.* **2016**, *128*, 10958–10963.
- [83] W. Zang, A. Sumboja, Y. Ma, H. Zhang, Y. Wu, S. Wu, H. Wu, Z. Liu, C. Guan, J. Wang, S. J. Pennycook, *ACS Catal.* **2018**, *8*, 8961–8969.
- [84] S. Gong, C. Wang, P. Jiang, L. Hu, H. Lei, Q. Chen, *J. Mater. Chem. A* **2018**, *6*, 13254–13262.
- [85] Q. Lai, Y. Zhao, J. Zhu, Y. Liang, J. He, J. Chen, *ChemElectroChem* **2018**, *5*, 1822–1826.
- [86] Y. Yang, K. Mao, S. Gao, H. Huang, G. Xia, Z. Lin, P. Jiang, C. Wang, H. Wang, Q. Chen, *Adv. Mater.* **2018**, *30*, 1801732.
- [87] a) Y. Lee, J. Suntivich, K. J. May, E. E. Perry, Y. Shao-Horn, *J. Phys. Chem. Lett.* **2012**, *3*, 399–404; b) T. Y. Ma, S. Dai, M. Jaroniec, S. Z. Qiao, *J. Am. Chem. Soc.* **2014**, *136*, 13925–13931.
- [88] J.-S. Lee, G. Nam, J. Sun, S. Higashi, H.-W. Lee, S. Lee, W. Chen, Y. Cui, J. Cho, *Adv. Energy Mater.* **2016**, *6*, 1601052.
- [89] C. Lin, S. S. Shinde, Z. Jiang, X. Song, Y. Sun, L. Guo, H. Zhang, J.-Y. Jung, X. Li, J.-H. Lee, *J. Mater. Chem. A* **2017**, *5*, 13994–14002.
- [90] M. Khalid, A. M. B. Honorato, H. Varela, L. Dai, *Nano Energy* **2018**, *45*, 127–135.
- [91] Y. Jiang, Y.-P. Deng, J. Fu, D. U. Lee, R. Liang, Z. P. Cano, Y. Liu, Z. Bai, S. Hwang, L. Yang, D. Su, W. Chu, Z. Chen, *Adv. Energy Mater.* **2018**, *8*, 1702900.
- [92] F. Meng, H. Zhong, D. Bao, J. Yan, X. Zhang, *J. Am. Chem. Soc.* **2016**, *138*, 10226–10231.
- [93] S. H. Ahn, A. Manthiram, *Small* **2017**, *13*, 1702068.
- [94] Z. Guo, F. Wang, Y. Xia, J. Li, A. G. Tamirat, Y. Liu, L. Wang, Y. Wang, Y. Xia, *J. Mater. Chem. A* **2018**, *6*, 1443–1453.
- [95] Y. Hao, Y. Xu, W. Liu, X. Sun, *Mater. Horiz.* **2018**, *5*, 108–115.
- [96] T. Meng, J. Qin, S. Wang, D. Zhao, B. Mao, M. Cao, *J. Mater. Chem. A* **2017**, *5*, 7001–7014.
- [97] Y.-N. Chen, Y. Guo, H. Cui, Z. Xie, X. Zhang, J. Wei, Z. Zhou, *J. Mater. Chem. A* **2018**, *6*, 9716–9722.
- [98] J. Li, S. Lu, H. Huang, D. Liu, Z. Zhuang, C. Zhong, *ACS Sustainable Chem. Eng.* **2018**, *6*, 10021–10029.
- [99] X. Song, S. Chen, L. Guo, Y. Sun, X. Li, X. Cao, Z. Wang, J. Sun, C. Lin, Y. Wang, *Adv. Energy Mater.* **2018**, *8*, 1801101.
- [100] I. S. Amiinu, Z. Pu, X. Liu, K. A. Owusu, H. G. R. Monestel, F. O. Boakte, H. Zhang, S. Mu, *Adv. Funct. Mater.* **2017**, *27*, 1702300.
- [101] X. Wu, G. Meng, W. Liu, T. Li, Q. Yang, X. Sun, J. Liu, *Nano Res.* **2018**, *11*, 163–173.
- [102] H. Liu, M.-Q. Wang, Z.-Y. Chen, H. Chen, M.-W. Xu, S.-J. Bao, *Dalton Trans.* **2017**, *46*, 15646–15650.
- [103] J. Zhang, X. Song, P. Li, S. Wang, Z. Wu, X. Liu, *Catalysts* **2018**, *8*, 243.

- [104] Y. Ye, F. Cai, C. Yan, Y. Li, G. Wang, X. Bao, *J. Energy Chem.* **2017**, *26*, 1174–1180.
- [105] M. Wang, T. Qian, J. Zhou, C. Yan, *ACS Appl. Mater. Interfaces* **2017**, *9*, 5213–5221.
- [106] W. Yang, Y. Zhang, X. Liu, L. Chen, J. Jia, *Chem. Commun.* **2017**, *53*, 12934–12937.
- [107] H. Zou, B. He, P. Kuang, J. Yu, K. Fan, *ACS Appl. Mater. Interfaces* **2018**, *10*, 22311–22319.
- [108] Y. Li, W. Zhou, J. Dong, Y. Luo, P. An, J. Liu, X. Wu, G. Xu, H. Zhang, J. Zhang, *Nanoscale* **2018**, *10*, 2649–2657.
- [109] C. Xuan, J. Wang, W. Xia, J. Zhu, Z. Peng, K. Xia, W. Xiao, H. L. Xin, D. Wang, *J. Mater. Chem. A* **2018**, *6*, 7062–7069.
- [110] J. Wang, Z. Wu, L. Han, R. Lin, W. Xiao, C. Xuan, H. L. Xin, D. Wang, *J. Mater. Chem. A* **2016**, *4*, 5678–5684.
- [111] a) A. Ajaz, N. Fujiwara, Q. Xu, *J. Am. Chem. Soc.* **2014**, *136*, 6790–6793; b) P. Zhang, F. Sun, Z. Xiang, Z. Shen, J. Yun, D. Cao, *Energy Environ. Sci.* **2014**, *7*, 442–450.
- [112] Y. Qian, T. An, K. E. Birgersson, Z. Liu, D. Zhao, *Small* **2018**, *14*, 1704169.
- [113] M. Yang, X. Hu, Z. Fang, L. Sun, Z. Yuan, S. Wang, W. Hong, X. Chen, D. Yu, *Adv. Funct. Mater.* **2017**, *27*, 1701971.
- [114] Y. Wang, L. Tao, Z. Xiao, R. Chen, Z. Jiang, S. Wang, *Adv. Funct. Mater.* **2018**, *28*, 1705356.
- [115] C. Xuan, B. Hou, W. Xia, Z. Peng, T. Shen, H. L. Xin, G. Zhang, D. Wang, *J. Mater. Chem. A* **2018**, *6*, 10731–10739.
- [116] Y. Li, Z. Yan, Q. Wang, H. Ye, M. Li, L. Zhu, X. Cao, *Electrochim. Acta* **2018**, *282*, 224–232.
- [117] Y. Qian, Z. Hu, X. Ge, S. Yang, Y. Peng, Z. Kang, Z. Liu, J. Y. Lee, D. Zhao, *Carbon* **2017**, *111*, 641–650.
- [118] J. Guo, B. Ghen, Q. Hao, J. Nie, G. Ma, *Appl. Surf. Sci.* **2018**, *456*, 959–966.
- [119] J.-T. Ren, G.-G. Yuan, C.-C. Weng, Z.-Y. Yuan, *ACS Sustainable Chem. Eng.* **2018**, *6*, 707–718.
- [120] H. Han, S. Chao, Z. Bai, X. Wang, X. Yang, J. Qiao, Z. Chen, L. Yang, *ChemElectroChem* **2018**, *5*, 1868–1873.
- [121] S. Hu, T. Han, C. Lin, W. Xiang, Y. Zhao, P. Gao, F. Du, X. Li, Y. Sun, *Adv. Funct. Mater.* **2017**, *27*, 1700041.
- [122] J. Tang, R. R. Salunkhe, J. Liu, N. L. Torad, M. Imura, S. Furukawa, Y. Yamauchi, *J. Am. Chem. Soc.* **2015**, *137*, 1572–1580.
- [123] Y.-Z. Chen, C. Wang, Z.-Y. Wu, Y. Xiong, Q. Xu, S.-H. Yu, H.-L. Jiang, *Adv. Mater.* **2015**, *27*, 5010–5016.
- [124] N. S. Kim, Y. T. Lee, J. Park, J. B. Han, Y. S. Choi, S. Y. Choi, J. Choo, G. H. Lee, *J. Phys. Chem. B* **2003**, *107*, 9249–9255.
- [125] a) H. Wang, Q.-L. Zhu, R. Zou, Q. Xu, *Chem* **2017**, *2*, 52–80; b) X.-F. Lu, P.-Q. Liao, J.-W. Wang, J.-X. Wu, X.-W. Chen, C.-T. He, J.-P. Zhang, G.-R. Li, X.-M. Chen, *J. Am. Chem. Soc.* **2016**, *138*, 8336–8339.
- [126] B.-Q. Li, S.-Y. Zhang, B. Wang, Z.-J. Xia, C. Tang, Q. Zhang, *Energy Environ. Sci.* **2018**, *11*, 1723–1729.
- [127] G. Chen, J. Zhang, F. Wang, L. Wang, Z. Liao, E. Zschech, K. Müllen, X. Feng, *Chem. Eur. J.* **2018**, in press. DOI: 10.1002/chem.201804339.
- [128] L. Zhu, D. Zheng, Z. Wang, X. Zheng, P. Fang, J. Zhu, M. Yu, Y. Tong, X. Lu, *Adv. Mater.* **2018**, *1805268*, in press, DOI: 10.1002/adma.201805268.

Manuscript received: September 14, 2018

Version of record online: November 14, 2018